AGU PUBLICATIONS

JGR

Journal of Geophysical Research: Atmospheres

RESEARCH ARTICLE
10.1002/2016JD025184

Key Points:
- Forest cover reduction decreases snow sublimation from both the canopy and snowpack at the basin scale
- Forest cover reduction only increases snowpack sublimation for conditions supporting long snowpack duration
- Snowpack sublimation increase overcomes canopy sublimation decrease upon forest reduction in dense, high, south aspect forest in wet years

Supporting Information:
- Supporting Information S1

Correspondence to:
B.M. Svoma,
svomab@missouri.edu

Citation:
Svoma, B. M. (2017), Canopy effects on snow sublimation from a central Arizona Basin, *J. Geophys. Res. Atmos.*, *122*, 20–46, doi:10.1002/2016JD025184.

Received 4 APR 2016
Accepted 3 DEC 2016
Accepted article online 9 DEC 2016
Published online 4 JAN 2017

Canopy effects on snow sublimation from a central Arizona Basin

Bohumil M. Svoma[1]

[1]Department of Soil, Environmental, and Atmospheric Sciences, University of Missouri, Columbia, Missouri, USA

Abstract Guided by 30 m terrain and forest cover data, snow sublimation from the Salt River basin in the Southwest U.S. is simulated for years 2008 (wet year) and 2007 (dry year). Downscaled meteorological input correlates well (r~0.80) with independent observations at AmeriFlux sites. Additionally, model correlation and bias with eddy-covariance vapor flux observations is comparable to previous localized modeling efforts. Upon a 30% reduction in effective leaf area index, canopy sublimation decreases by 1.29 mm (27.0%) and 1.05 mm (23.0%) at the basin scale for the 2008 and 2007 simulations, respectively. Ground sublimation decreases 0.72 mm (4.75%) in 2008 and only 0.17 mm (1.5%) in 2007. Canopy snow-holding capacity and frequent unloading events at lower elevations limit the variability in canopy sublimation from wet year to dry year at the basin scale. The greater decrease in snowpack sublimation in the wet year is partly due to decreased longwave radiation from the canopy reduction over a more extensive snowpack than the dry year. This decrease overcomes the increased solar radiation and wind speed during winter. A second factor is that a greater extent of the snowpack persisted into spring in 2008 than 2007, and the large increase in shortwave flux upon canopy reduction increases melt rates, reducing duration. Only in heavily forested high elevations (>2900 m above sea level) in 2008 does the snowpack persist long enough into spring to result in increased ground sublimation upon canopy reduction. As forest cover change can occur rapidly, these results are critical from water resource and ecosystem function perspectives.

1. Introduction

Sublimation of snow cover is a phase change from ice to water vapor and directly affects snow accumulation, impacting ecosystem processes, soil moisture, soil porosity, biogeochemical processes, wildfire, and water resources [*Barnett et al*., 2005; *LaMalfa and Ryle*, 2008; *Broxton et al*., 2014]. When snowfall is intercepted by vegetation and sublimates before being unloaded to the ground snowpack, canopy (or intercepted) sublimation occurs [*Molotch et al*., 2007]. Snow stored in the canopy has a high surface area to mass ratio and is often exposed to high-energy conditions (e.g., high wind speed and solar radiation), leading to generally increased sublimation rates relative to the ground snowpack [*Pomeroy et al*., 1998; *Strasser et al*., 2008]. Compared to the snowpack in open areas, the subcanopy environment is more sheltered and typically experiences reduced shortwave radiation and wind speeds as well as increased humidity and longwave radiation; thus, the forest canopy impacts ground (or snowpack) sublimation [*Pomeroy et al*., 1998; *Strasser et al*., 2008].

Jackson and Prowse [2009] present a table of sublimation rates from more than 30 previous investigations. Wind-exposed alpine environments generally produce high rates of ground sublimation (e.g., a mean of 2 mm d^{-1} from *Marks and Dozier* [1992] and 0.9–1.8 mm d^{-1} from *Hood et al*. [1999]). Open areas tend to experience more rapid ground sublimation than adjacent forested areas, for example, 1.0 mm d^{-1} (subcanopy) versus 2.0 mm d^{-1} (open) from *Suzuki et al*. [2006] and 0.35 mm d^{-1} (subcanopy) versus 0.45 mm d^{-1} (open) from *Kaitera and Teräsvirta* [1972]. In boreal forests, canopy sublimation rates are considerably larger than ground sublimation rates, with *Nakai et al*. [1999] reporting 1.2 mm d^{-1} for canopy sublimation and *Kaitera and Teräsvirta* [1972] reporting 0.45 mm d^{-1} in forest clearings. *Molotch et al*. [2007] measured canopy sublimation rates of 0.71 mm d^{-1} and subcanopy sublimation rates of 0.41 mm d^{-1} in a subalpine forest in Colorado, USA.

Sublimation rates also vary by season. An extreme example is reported by *Rylov* [1969], who find January sublimation rates of 0.08 mm d^{-1} and April rates of 0.6 mm d^{-1} in open areas of Kazakhstan. The increase in sublimation rate from winter to spring is more subtle as reported by other studies in the western United States [e.g., *Reba et al*., 2012; *Molotch et al*., 2009; *Sexstone et al*., 2016], and *Hood et al*. [1999] found that rates of sublimation decreased from winter to spring at an alpine site in Colorado, USA. *Hood et al*. [1999] attributed this to the higher wind speeds during the winter and the higher humidity of late spring.

Measurement techniques for sublimation have challenges and uncertainty. The eddy-covariance (EC) measurement technique requires high-frequency observations from sonic anemometers and infrared gas analyzers [*Hood et al*., 1999]. EC measurements at multiple levels are required to separate ground sublimation from canopy sublimation, which has proven to be difficult [*Mahat et al*., 2013]. Additionally, transpiration and vapor flux from areas without snow cover cannot be separated from snow sublimation through the EC method [*Molotch et al*., 2009]. Inaccuracies from gravimetric techniques (e.g., tree weighing) arise from the occurrence of precipitation, snow removal by wind, and from sampling a snow surface with properties that are not representative of the surroundings [*Schmidt et al*., 1998; *Lundberg and Halldin*, 2001]. Measurements of ion chemistry and water isotopes have been used to estimate snow sublimation [*Koeniger et al*., 2008; *Gustafson et al*., 2010; *Ohlanders et al*., 2013]. These methods are labor intensive and difficult to apply over long time periods and large domains [*Ohlanders et al*., 2013]. Total vapor loss from a watershed can be estimated from accurate measurements of stream discharge and spatially distributed precipitation assuming, a negligible change in terrestrial water storage, but the quantification of evaporation and transpiration during warm periods is required to isolate snow sublimation [*Svoma*, 2016].

Models are therefore promising tools to produce spatially distributed estimates of sublimation. Canopy snow interception-sublimation, unloading from the canopy, and the canopy alteration of the energy budget over the snowpack are all essential components of snow models suitable for forested environments. While an exhaustive review of each of these model components is beyond the scope of this Introduction, it is important to highlight several different components related to sublimation flux. Previous investigators have represented sublimation processes with varying complexity. For example, interception components that require only effective leaf area index [*Liston and Elder*, 2006b] to those that additionally require total gap area and mean distance to canopy [*Moeser et al*., 2016]. For canopy sublimation, ice-sphere models [*Thorpe and Mason*, 1966; *Liston and Elder*, 2006b; *Strasser et al*., 2011] commonly assume that canopy temperature is equal to the air temperature, while others track the temperature of intercepted snow through coupling the canopy energy budget with the snowpack energy budget [*Mahat et al*., 2013]. While snowpack turbulent vapor flux equations that assume medium roughness and stable stratification have been employed [*Strasser et al*., 2008], other investigators have used flux equations with stability adjustments and surface roughness length as a tunable parameter [*Mahat et al*., 2013; *Reba et al*., 2014].

Estimates of sublimation are spatially distributed through modeling but have largely been restricted to high latitudes [*Van den Broeke*, 1997; *Déry and Yau*, 2002; *Essery et al*., 2003; *Suzuki et al*., 2015] or to small spatial domains (e.g., ~100 km^2) in complex terrain [*Strasser et al*., 2008; *Strasser et al*., 2011; *Bernhardt et al*., 2012]. This is likely due in part to the necessity for high-resolution input of meteorological variables (e.g., radiation, precipitation, and temperature) and land cover variables (e.g., forest cover type and density). Furthermore, these distributed modeling efforts in mountainous terrain have been focused on nonarid climates in the upper midlatitudes.

Forest cover density controls total interception and thus canopy sublimation [*Boon*, 2012; *Pugh and Small*, 2013; *Biederman et al*., 2014]. However, the portion of snowfall intercepted is also controlled by snowfall intensity, and because of the limiting effects of canopy snow-holding capacity, heavy snow years may not lead to a proportional increase in intercepted snowfall [*Boon*, 2012]. In addition, canopy sublimation is also controlled by the duration of canopy snow storage with cold and/or snowy environments often experiencing nearly continuous canopy snow storage and drier temperate environments experiencing intermittent storage [*Yamazaki et al*., 2007; *Suzuki and Nakai*, 2008].

Variations in total ground sublimation with forest cover density are more complex. For example, decreased interception from decreased forest cover density can lead to increased peak snow water equivalent [*Broxton et al*., 2014] or SWE. However, changes in absorbed solar radiation affect peak SWE and melt rates [*Rinehart et al*., 2008], and reduced snowpack duration may result from decreased forest density, which could ultimately decrease total ground sublimation [*Molotch et al*., 2009; *Mahmood and Vivoni*, 2014; *Perrot et al*., 2014]. *Lundquist et al*. [2013] show that in regions with an average winter temperature greater than −1°C, forest cover generally reduces snow cover duration compared to adjacent open areas.

The trade-off between increased sublimation rate and melt rate is also affected by wind speed and longwave radiation. *Biederman et al*. [2014] speculate that increased wind speed could have contributed to increased winter ground sublimation in response to reduced forest density. *Harpold et al*. [2014] suggest that ground

sublimation in regions with relatively high solar elevation angles and many cloud-free days would be particularly sensitive to increased shortwave radiation upon the removal of the canopy by wildfire. Longwave radiation is also important to the snowpack energy budget [*Meromy et al*., 2015; *Gouttevin et al*., 2015]. Changes in forest cover density may result in greater changes in incoming longwave radiation than changes in shortwave radiation during conditions of low solar elevation angle, low atmospheric emissivities, and high snow albedos [*Lundquist et al*., 2013].

The available energy, the exposed surface area of a snow cover, and exposure time with the atmosphere vary greatly with aspect, elevation, forest cover, latitude, and continentality [*Rinehart et al*., 2008; *Pugh and Small*, 2013; *Mahmood and Vivoni*, 2014; *Broxton et al*., 2014; *Harpold et al*., 2014]. Therefore, sublimation rates and snow cover duration exhibit high variability in complex forested terrain [*Schmidt et al*., 1998; *Molotch et al*., 2007; *Reba et al*., 2012; *Mahmood and Vivoni*, 2014]. It is difficult to scale up results from site-specific short-term observational studies [*Jackson and Prowse*, 2009]. Forest cover properties can vary considerably on short and long time scales through natural (wildfire, bark beetle infestation, and drought) and anthropogenic (land management practices) processes [*La Malfa and Ryle*, 2008; *Pugh and Small*, 2013]. Therefore, understanding how small-scale changes impact snow sublimation at larger spatial scales, and how this varies temporally, is critical from ecosystem function and water resource perspectives.

The goal of this investigation is to determine the forest cover effects, and the variability thereof, on canopy and ground sublimation from a large, forested, lower midlatitude basin. Canopy and ground sublimation are simulated for a wet year and a dry year over the Salt River basin in central Arizona. The three hypotheses are (1) decreasing forest cover decreases ground sublimation for conditions favoring short duration in spring. For example, at low to middle elevations of the snowpack, forest cover sheltering effects will extend snowpack duration beyond late winter, increasing total ground sublimation relative to less sheltered areas due to the increased duration. In contrast, with general conditions promoting duration long into spring (e.g., wet years at high elevation) forest cover sheltering will reduce ground sublimation. (2) Due to a more widespread and persistent snowpack during the wet year, the effects of forest cover on ground sublimation will be greater at the basin scale for the wet year than the dry year. (3) Forest cover reduction will reduce canopy sublimation more for the wet than the dry year, but the wet year to dry year difference will be less than for ground sublimation at the basin scale because of the limiting effects of canopy snow-holding capacity and unloading.

2. Study Area

The Salt River basin (Figure 1) is highly managed with a series of four reservoirs and nearly 2.5×10^9 m^3 of storage, accounting for a substantial portion of the metropolitan Phoenix, Arizona, water supply [*Ellis et al*., 2008]. Above the confluence of the Salt and the Verde Rivers near metropolitan Phoenix, the Salt River basin is ~16,200 km^2 in land area [*Baker et al*., 1998]. At the confluence, the elevation is 425 m above sea level (asl) with the highest point in the basin above 3450 m asl [*Baker et al*., 1998; *Fassnacht et al*., 2001; *Molotch et al*., 2004]. Annual precipitation across the arid metropolitan Phoenix is about 200 mm yr^{-1}, yet the higher elevations of the Salt receive over 800 mm yr^{-1} annually [*Baker et al*., 1998; *Bolin et al*., 2010]. Thirty-nine percent of annual precipitation at Snowpack Telemetry (SNOTEL) sites in central Arizona occurs as snowfall and more than half of the runoff is generated from snowpack that is generally established above 2200 m asl [*Baker et al*., 1998; *Molotch et al*., 2004]. SNOTEL sites in Arizona and southern New Mexico display an average date of peak snow water equivalent (SWE) on 20 February with more than 160 mm average peak SWE and an average snowpack disappearance of 8 May [*Serreze et al*., 1999]. The subalpine zone in the region ranges from 3050 m asl to 3500 m asl [*Cooper*, 1987]. Forested regions in central Arizona are predominantly ponderosa pine with mixed conifer above ~2600 m asl [*Adams and Kolb*, 2004; *Ganey and Vojta*, 2011].

3. Data and Methods

3.1. Meteorological Input

Meteorological input is guided by four data sets ranging in resolution from 32 km to 30 m (Figure 2). Variable and acronym descriptions relevant to Figure 2 are displayed in Table 1. The 32 km North American Regional Reanalysis (NARR) data [*Mesinger et al*., 2006] are first adjusted for terrain (Figure 2), with the 4 km daily Parameter-elevation Regression on Independent Slopes Model (PRISM) data providing an intermediate step

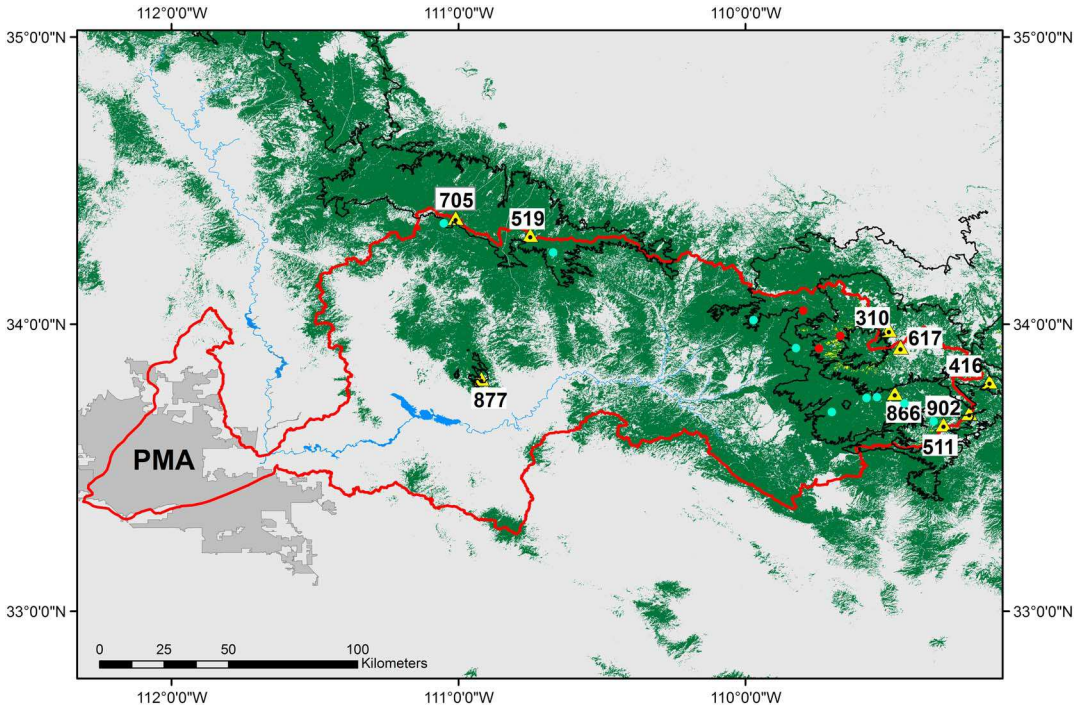

Figure 1. The Salt River drainage basin boundary (red lines); the Phoenix Metropolitan Area (PMA; gray polygon) in central Arizona, USA; and the 2100, 2500, and 2900 m asl contour lines (black lines). Also displayed are evergreen forests (green), deciduous forests (yellow; almost entirely between 2500 and 2900 m asl in the eastern portion of the watershed), rivers and reservoirs (blue), SNOTEL sites (yellow triangles), locations of targeted simulations displayed in sections 4.4.3–4.4.5 (red dots), and locations of targeted simulations not displayed in this paper (teal dots).

for temperature, specific humidity, and precipitation. More details of the terrain adjustment methods are given in Text S1 in the supporting information.

The terrain/PRISM adjusted data are then adjusted for forest cover (evergreen, deciduous, and mixed) based on LAI*, the effective leaf area index (Figure 2). For model validation at the flux tower sites discussed in section 4.2, an LAI* for each local 30 m cell was determined by multiplying the reported LAI* in the literature [*Molotch et al*., 2007; *McDowell et al*., 2008] by the National Land Cover Data (NLCD) 2011 canopy cover fraction as in *Broxton et al*. [2014]. For Salt River basin (Figure 1) simulations, simple linear regression was used to determine LAI* based on measured LAI* from 17 separate ponderosa pine plots presented by *Law et al*. [2001] and from NLCD 2011 canopy cover percentage (CC). The regression equation is

$$\mathrm{LAI}^* = 0.03194 \times \mathrm{CC} + 0.0717 \quad (1)$$

where canopy cover percentage is from the NLCD 2011. On the Salt, the maximum CC is 73% (LAI* = 2.403 from equation (1)), and there are no occurrences of CC less than 4% (LAI* = 0.1995 from equation (1)). The regression LAI* was scaled for deciduous and mixed NLCD 2011 forest types based on the table of forest type parameterizations given by *Liston and Elder* [2006b]; e.g., LAI* for deciduous is 20% of coniferous forest. For the ground snowpack in forested areas, the minor adjustments to temperature and humidity by *Liston and Elder* [2006b] and *Strasser et al*. [2011] are utilized (Figure 2). The terrain-adjusted shortwave flux (see Text S1) from NARR is reduced by *Liston and Elder* [2006b]:

$$Q_{si} = Q_{siT} e^{-k \cdot \mathrm{LAI}^*} \quad (2)$$

where Q_{siT} is the terrain-adjusted shortwave flux (Figure 2) and k is an extinction coefficient taken to be 0.71, as in SnowModel [*Liston and Elder*, 2006b]. The terrain-adjusted incoming longwave flux (Q_{liT}) from NARR is adjusted by *Liston and Elder* [2006b]:

$$Q_{li} = (1 - F_c) Q_{liT} + F_c \sigma T_c^4 \quad (3)$$

$$F_c = 0.55 + 0.29 \ln (\mathrm{LAI}^*) \quad (4)$$

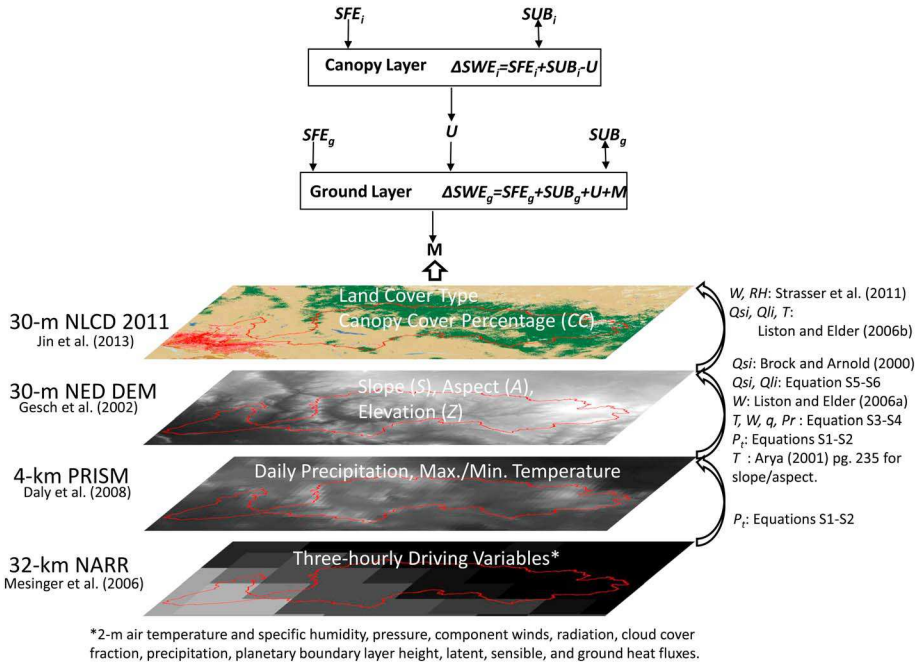

Figure 2. Modeling flowchart and source information. See Table 1 for the descriptions of variables and acronyms. Equations are found in the supporting information document. See references *Arya* [2001], *Brock and Arnold* [2000], *Daly et al.* [2008], *Gesch et al.* [2002], *Jin et al.* [2013], and *Liston and Elder* [2006a].

where T_c is the canopy temperature. T_c is assumed to be equal to the air temperature over the snowpack [*Liston and Elder*, 2006b], and σ is the Stefan-Boltzmann constant (Table 2).

3.2. The Snowpack Model System

Spatially distributed modeling studies in complex terrain [*Strasser et al.*, 2008; *Suzuki et al.*, 2011; *Bernhardt et al.*, 2012; *Groot Zwaaftink et al.*, 2013] find blowing snow sublimation to be a significant contribution to the seasonal water budget for isolated portions of alpine areas, although a notably smaller contribution than ground sublimation over broader areas [e.g., *Groot Zwaaftink et al.*, 2013]. However, if the watershed is predominately not alpine, blowing snow sublimation has been found to be a small contribution to the water budget by these studies, e.g., 0.2%–4.1% of total snowfall [*Strasser et al.*, 2008; *Suzuki et al.*, 2011; *Bernhardt et al.*, 2012; *Groot Zwaaftink et al.*, 2013]. Therefore, blowing snow sublimation is not considered in this study.

The snow mass balance for snowpack and interception-unloading-sublimation models are given in Figure 2. Relevant model parameters are presented in Table 2, and the most relevant aspects of the models are discussed below, with more details in Text S2. The *Hedstrom and Pomeroy* [1998] snowfall interception model was used, and sublimation from the canopy was determined from the ice-sphere model for canopy sublimation presented by *Pomeroy et al.* [1998]. This interception-sublimation model process is discussed in detail by *Liston and Elder* [2006b]. The terrain-adjusted temperature and humidity (Figure 2 and Text S1) are used to calculated canopy sublimation [*Liston and Elder*, 2006b]. After, terrain adjustment to wind (Figure 2), the wind speed for calculating canopy sublimation is determined as a function of LAI^*, as in *Strasser et al.* [2011]. The albedo of the snow in the canopy is assumed to be the same albedo as the ground snowpack [*Strasser et al.*, 2011].

Canopy sublimation (SUB_i) rate (kg m^{-2} s^{-1}) for the ice-sphere model is given by *Pomeroy et al.* [1998] and *Liston and Elder* [2006b]:

$$\mathrm{SUB}_i = I\frac{dm/dt}{m}k_c\left(\frac{I}{I_{\max}}\right)^{-0.4} \tag{5}$$

where I is the intercepted snow load (kg m^{-2}), $I_{\max}$ is the maximum snow load (kg m^{-2}) given by $4.4 \times \mathrm{LAI}^*$, k_c is a dimensionless coefficient to account for the shape of snow deposits in the canopy (assumed to be 0.010

Table 1. Descriptions of Acronyms and Variables Used in Figure 2 and Commonly in the Text

Variable/Acronym	Description
A	aspect
CC	canopy cover percentage from NLCD 2011
DEM	digital elevation model
asl	above sea level
M	melt flux
NARR	North American Regional Reanalysis
NLCD	National Land Cover Database
LAI^*	effective leaf area index
NED	National Elevation Data Set
P_t	precipitation flux (at time step t)
Pr	atmospheric pressure
PRISM	Parameter-elevation Regression on Independent Slopes Model data set
q	specific humidity
Q_{si}	downward solar radiation flux
Q_{li}	downward longwave radiation flux
RH	relative humidity
S	slope
SFE_i	snowfall liquid equivalent intercepted
SFE_g	snowfall liquid equivalent not intercepted
SUB_i	intercepted (canopy) sublimation
SUB_g	ground (snowpack) sublimation
SWE_i	snow water equivalent of canopy snow load
SWE_g	snow water equivalent of the snowpack
T	air temperature
U	canopy to ground snow unloading flux
W	wind speed
Z	land elevation

here), and dm/dt is the mass change in time (s) of an ice sphere of mass m (kg). A more complete description of equation (5) is given in Text S2.

Ground sublimation (SUB_g) rate (kg m^{-2} s^{-1}) is given by *Strasser et al.* [2008], assuming stable stratification and medium roughness:

$$SUB_g = \frac{1}{h_s} 32.82 \cdot (0.18 + 0.098 \cdot W) \cdot (e - e_s(T_s)) \quad (6)$$

where W is the wind speed (m s^{-1}), h_s is the latent heat of sublimation (J kg^{-1}), e is the vapor pressure (hPa), and e_s is the saturation vapor pressure with respect to ice (hPa) at the snow surface temperature (T_s) as in *Liston and Elder* [2006b]. More details of the model snowpack energy balance [*Luce and Tarboton*, 2010; *Mahat et al.*, 2013] are given in Text S2.

Table 2. Values of Relevant Model Parameters

Values	Basis
Temperature that precipitation is all snowfall, −1°C	*Mahat et al.* [2013]
Temperature that precipitation is all rainfall, 3°C	*Mahat et al.* [2013]
LAI^* at Flagstaff Unmanaged Forest AmeriFlux site, 2.2 ± 0.7	*Dore et al.* [2010]
LAI^* at Valles Caldera Mixed Conifer AmeriFlux site, 3.09 ± 0.5	*McDowell et al.* [2008]
Maximum snowpack density, 550.0 kg m^{-3}	*Liston and Hall* [1995]
Soil heat flux (Q_g), 2.0 W m^{-2}	*Strasser et al.* [2011]
Emissivity of snow (ε_s), 0.99	*Strasser and Marke* [2010]
Stefan-Boltzmann constant (σ), 5.67×10^{-8} W m^{-2} K^{-4}	*Strasser and Marke* [2010]
Specific heat of ice (c_i), 2.09 kJ kg^{-1} K^{-1}	*Luce and Tarboton* [2010]
Specific heat of water (c_w), 4.2 kJ kg^{-1} K^{-1}	*Strasser and Marke* [2010]
Latent heat of sublimation (h_s), 2834 kJ kg^{-1}	*Mahat et al.* [2013]
Latent heat of melting, 333.7 kJ kg^{-1}	*Strasser et al.* [2011]
Angular frequency of a diurnal forcing (ω), 0.2618 h^{-1}	*Luce and Tarboton* [2010]
Maximum canopy snow storage, $4.4 \times LAI^*$	*Liston and Elder* [2006b]
Model time step (Δt), 3 h	NARR temporal resolution

3.3. Validation

Since accurate snow cover duration is important for simulating total ground sublimation for the snow season, the local area 30 m cell median of SWE was compared to observed SWE at nine SNOTEL sites (Figure 1) within and near the Salt for 2007 (dry year), 2008 (wet year), and 2009 (slightly above average precipitation with a long midwinter dry period). Interactive maps of SNOTEL locations are provided by Natural Resources Conservation Services website (http://www.wcc.nrcs.usda.gov/snow/). Used in conjunction with Google Earth, aerial imagery around the nine SNOTEL sites was examined. The sites tended to be adjacent to heavily forested areas to the south (commonly within ~15 m). Therefore, observations are also compared to "sheltered" simulations, where no snowfall is intercepted by the canopy, yet a 20 m tall forest within 15 m of the snow pillow is assumed to block all direct shortwave radiation when the solar zenith angle is larger than 36.9°. SNOTEL sites are often located in favorable locations for snow accumulation and long snowpack duration (e.g., small forest clearings in locally high-precipitation areas), and therefore, one should generally expect SWE observations at SNOTEL sites to be greater than the local area average [*Salzmann and Mearns*, 2012]. Therefore, if the model perfectly simulated the evolution of SWE, one might expect the sheltered simulations to generally display longer snow cover duration than observed and "nonsheltered" simulations to display shorter snow cover duration. Furthermore, *Mahat and Tarboton* [2014] report substantially more measured SWE than measured precipitation at SNOTEL sites, likely from wind redistribution of canopy intercepted snow which is most important at small spatial scales, a process neglected in the model system used here.

In snow seasons 2007 and 2008, nearly continuous 30 min water vapor flux and meteorological observations were available from the AmeriFlux Site and Data Exploration System (http://ameriflux.ornl.gov/) for the Flagstaff Unmanaged Forest (FUF) AmeriFlux tower, in Arizona (35.089°N, 111.769°W). This site is approximately 90 km northwest of the northwestern boundary of the Salt watershed. At 2180 m asl, the tower is within ponderosa pine forest. Because much of the Salt is above this elevation (Figure 1), data from the Valles Caldera Mixed Conifer (VMC) AmeriFlux tower were also obtained for snow seasons 2008–2010. The tower is 3003 m asl in the Jemez Mountains of New Mexico (35.888°N, 106.532°W), an arid lower latitude climate similar to the Salt.

An open-path LI-7500 (LI-COR Inc.) and CSAT-3 (Campbell Scientific) 3-D sonic anemometer at 21.65 m measurement height were used to determine water vapor flux at the VMC site with the EC technique [*Molotch et al*., 2009]. At the FUF site, a closed-path LI-7000 (LI-COR Inc.) and CSAT-3 (Campbell Scientific) 3-D sonic anemometer at 23 m measurement heights were used [*Dore et al*., 2008]. The canopy height surrounding the towers was 18 m and 19.6 m at the FUF and VMC sites, respectively [*Dore et al*., 2008; *Molotch et al*., 2009]. Flux parameters were sampled at 10 Hz, and details about data quality control, computation of means, gap filling, coordinate rotation, correction for frequency losses, density corrections, sonic temperature correction, and despiking are given in *Dore et al*. [2008], *Molotch et al*. [2009], *Schotanus et al*. [1983], *Aubinet et al*. [2000], and *Foken and Wichura* [1996]. Quality-controlled EC measurements have been used to validate above-canopy and below-canopy fluxes over snow-covered surfaces by several studies [e.g., *Molotch et al*., 2007; *Marks et al*., 2008; *Mahat et al*., 2013].

Figures from *Sogachev et al*. [2004] suggest that ~95% of the source contribution for vapor flux measured at 24 m in height is within an upwind range of 600 m in complex heterogeneous forested terrain. AmeriFlux observations were compared to average model meteorological input and simulated sublimation for 30 m cells within 600 m from the towers. Because wind direction is highly variable, simulations were for a circular area 600 m in radius. The flux footprint is highly dynamic and complex in shape [*Sogachev et al*., 2004; *Vivoni et al*., 2014]; however, it is important to note that the general agreement between observed fluxes and sublimation modeled was not highly sensitive to a range of reasonable footprint shapes and sizes. It is possible for portions of the AmeriFlux tower EC footprint to be snow free while the modeled SWE is nonzero. To reduce this possibility, model sublimation was only compared to observations when modeled SWE was greater than 10 mm. In general, when compared to higher thresholds, sample size remained high for this threshold (i.e., 10 mm), especially for the Flagstaff Unmanaged Forest AmeriFlux site.

While validation is essential for lending confidence to results, because the model is applied over large spatial scales (Figure 1), model overtuning may occur through maximizing agreement between simulated flux and EC measured flux at these specific locations. Unfortunately, large-scale and spatially distributed observations of snow sublimation do not exist. Therefore, using the already established parameterizations by other investigators is more appropriate for this study.

3.4. Wet Year and Dry Year Simulations

Simulations were performed for snow seasons (October–June) 2007 (dry year) and 2008 (wet year). As determined from the PRISM data, total 15 November to 30 April precipitation at 2200 m asl ranged from 432 mm to 810 mm in 2008 and ranged from 174 mm to 336 mm in 2007. For climatological reference, the average 15 November to 30 April precipitation at the wettest (driest) SNOTEL site is approximately 577 mm (251 mm). From 15 November to 30 April, precipitation occurred on approximately 21% of the days in 2008 and 26% of the days in 2007. Therefore, precipitation intensity differences caused the disparity in precipitation total between the 2 years.

3.5. Large-Scale Modeling

Modeling the snowpack at the large spatial scale (>10,000 km^2) for each 30 m cell is computationally expensive. Thus, for each NARR cell, snow cover was modeled for discrete classes of aspect (A), slope (S), elevation (Z), canopy cover percentage (CC), forest cover type, and October–May precipitation total. All 30 m cells were divided into precipitation classes based on their encompassing PRISM cell with each class spanning a range equal to 10% of the median snow season precipitation for elevations between 2200 and 2300 m asl. This value provided reasonable resolution (less than ~5% error over most of the watershed that establishes a stable snowpack) while limiting computational time. The midpoints of the classes were used as model input and were chosen to minimize the number of precipitation classes. The cells were categorized by land cover type (evergreen, deciduous, mixed, and nonforest), and the forested 30 m cells were further categorized by discrete canopy cover classes ($0 \le CC < 20$, $20 \le CC < 30$, $30 \le CC < 40$, $40 \le CC < 50$, $50 \le CC < 60$, and $60 \le CC$ percent). All cells were further categorized into slope classes ($0 \le S < 7.5$, $7.5 \le S < 22.5$, $22.5 \le S < 47.5$, and $47.5 \le S$ degrees) and aspect classes in degrees clockwise from north ($342 \le A$ and $A < 18$, $18 \le A < 54$, $54 \le A < 90$,… $306 \le A < 342$°). Last, the 30 m cells were categorized into discrete elevation classes spanning 100 m.

The midpoints of the A, Z, and CC class bounds were used as model input. Exceptions to this are for the lowest CC class where 15% was input in the model because very few (0.12%) forested cells displayed CC < 10% and the highest CC class where 65% was the model input because 73% was the maximum CC in the watershed. The input values for the S classes were 2.5, 12.5, 32.5, and 62.5° because of a highly right skewed distribution.

3.6. Experimental Framework

To determine the impact of forest cover changes on total sublimation, simulations were performed with LAI* reduced by 30%. It is important to note that 10% and 20% changes in LAI* were also considered. These results are not shown here as the only notable large-scale difference from 30% reduction was a dampened response to LAI* change. A 30% reduction in LAI* over such a large area is not unreasonable in the short term, as the goal of the Four Forest Restoration Initiative by the U.S. Forest Service is to thin nearly the entire ponderosa pine stand in central Arizona [*Moreno et al*., 2016]. Maps from *Moreno et al*. [2016] suggest that projected decreases in basal area of more than 40% due to the thinning are common. The change in total sublimation due to changes in LAI* are likely to be very sensitive to the length of time that snow is stored in the model canopy and to the subcanopy wind speeds. Snow unloading rate and wind speed adjustments for forest cover are particularly uncertain aspects of snow modeling in forested terrain [e.g., *Hedstrom and Pomeroy*, 1998; *Mahat et al*., 2013]. *Liston and Elder* [2006b] consider snow unloading from the canopy only for air temperatures above the melting point given by

$$U = 5.8 \times 10^{-5} \cdot (T - 273.16)\Delta t \tag{7}$$

where T is the air temperature in K, U is the unloading in kg m^{-2}, and Δt is the model time step in seconds. In addition to unloading during melting conditions, *Gelfan et al*. [2004] considered unloading during cold conditions to be

$$U = I \left(1 - e^{-\beta \cdot \Delta t}\right) \tag{8}$$

where I is the intercepted snow load after sublimation and the coefficient $\beta = 6.425 \times 10^{-7}$ s^{-1} was determined by *Hedstrom and Pomeroy* [1998].

An exponential reduction of wind speed for subcanopy adjustment has been utilized by *Strasser et al*. [2011]:

$$W = W_t \cdot \exp(-0.36 \cdot \mathrm{LAI}^*) \tag{9}$$

while *Perrot et al*. [2014] utilized a linear subcanopy adjustment equation:

$$W = W_t \left(1 - 0.8 \frac{\mathrm{CC}}{100}\right) \tag{10}$$

where W_t is the terrain-adjusted wind speed (Figure 2). In this study, CC in equation (10) is from the NLCD 2011 and is related to LAI* using equation (1). Because values of CC greater than 70% are few in the Salt (0.00009%), equation (10) produces higher wind speeds than equation (9). In this study, both high sublimation (HSUB) and low sublimation (LSUB) simulations are performed. LSUB simulations utilize equations (7)–(9), and HSUB simulations utilize equations (7) and (10), excluding unloading when air temperatures are below freezing.

3.7. Targeted Simulations

To further address the hypotheses in section 1, detailed analyses of SUB_i and SUB_g were performed for local-scale simulations (i.e., 30 m) across the watershed (Figure 1) and across aspect, slope, LAI*, and elevation gradients. Although somewhat subjective, selected simulations for display in this paper are representative of the general results from all targeted simulations. More specifically, full LAI* and reduced LAI* (reduced by 30%) simulations were analyzed for selected low-, middle-, and high-elevation PRISM cells (Figure 1), 2200 m asl, 2500 m asl, and 2900 m asl, respectively. At these three elevations, simulations were analyzed for flat surfaces, south and north aspects with 32.5° slope, and for initial effective leaf area index values (LAI_o) of 0.87, 1.19, 1.51, and 2.47 (corresponding to NLCD CC of 25%, 35%, 45%, and 75% for NLCD evergreen forest, respectively; see equation (1)). The average of the LAI* distribution is approximately 1.19. An LAI* of 1.51 is nearer to the average at higher elevations (e.g., >2500 m asl). Therefore, LAI* = 0.87 represents lightly forested terrain. An LAI* of 2.47 is near the maximum LAI* and therefore represents the most heavily forested areas of the watershed.

4. Results

4.1. Validation with SNOTEL Observations

Model agreement with observations was best at SNOTEL site 902 in 2008, where observed SWE is within the range of modeled SWE from the sheltered and nonsheltered simulations for nearly the entire snow season (Figure 3). Agreement was poorest at SNOTEL site 877 in 2007, where the sheltered simulation failed to establish a stable snowpack until mid-January resulting in substantial low bias (Figure 3). In general, there was a tendency for duration to be underestimated in 2007 and overestimated in 2008 (Table 3), but the model appears to represent snow cover duration reasonably well, with 14 out of 26 simulation pairs (sheltered and nonsheltered), displaying longer duration than observed for sheltered and shorter duration than observed for nonsheltered simulations. These results are distributed evenly across the 3 years, with four in 2007 and five in 2008 and 2009. In addition, the duration of nonsheltered simulations is within 7 days of observed for 10 out of 26 instances (Table 3).

In general, there is a tendency for low bias in simulated SWE (Table 3). This is due to the underestimation of peak SWE (not shown), which is possibly a result of the coarseness of the precipitation data (~4 km) or snow redistribution by wind at the SNOTEL site. An exception is for water year 2008 for the four lowest elevation SNOTEL sites (705, 877, 866, and 519), where there is an overestimation of peak SWE leading to large positive SWE biases throughout the snow season (Table 3). As these sites are lower in elevation, simulated total snowfall there is very sensitive to simulated rain/snow fraction driven by temperature (Table 2). For example, there is a less than 10% low bias in total precipitation at these SNOTEL sites in 2008, suggesting good agreement between precipitation input into the snow model and precipitation observed at these SNOTEL sites. It should be noted, however, that the PRISM data set assimilates SNOTEL records, and these are not independent comparisons. Despite the biases in rain/snow fraction, it is important to note that duration is only substantially overestimated at two sites in 2008, 705 and 866 (Table 3).

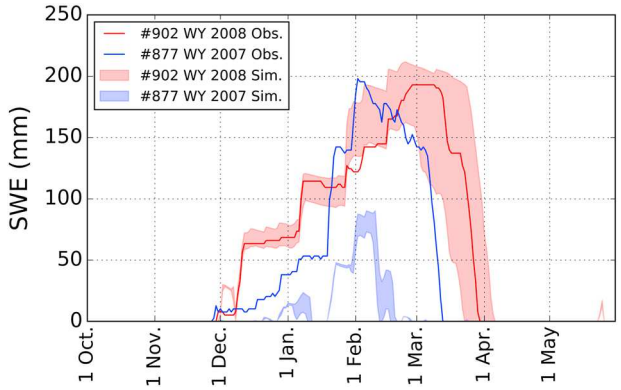

Figure 3. The envelope for sheltered and nonsheltered simulations of SWE for SNOTEL site 902 (red shading) and SNOTEL site 877 (blue shading). Observed SWE is given by the red line (902) and the blue line (877).

4.2. Validation at AmeriFlux Sites

Agreement between adjusted NARR data for terrain only (Figure 2 and Text S1) and AmeriFlux observations is best for air temperature, with correlations (r) ranging from 0.78 to 0.88 with a cold bias tendency at the FUF site and a slight warm bias at the VMC site (Table 4). Agreement correlations for relative humidity range from 0.65 to 0.79 with a bias toward higher humidity values but generally within 5%. Correlation coefficients for wind speed are lower, ranging from 0.32 to 0.61, and notably lower for the VMC site (Table 4). One would expect high wind speed bias, as the instrumentation on the towers are only ~2 m and ~5 m above the canopy at the VMC and FUF sites, respectively [*Dore et al*., 2008; *Molotch et al*., 2009], and the NARR provides winds at 10 m. There is good agreement between seasonal totals of observed precipitation and precipitation input into the model (Table 4). This is

Table 3. For the Salt River Watershed (Figure 1), Agreement Measures Between Observed and Simulated SWE

			Snow-Free Date Difference (Days)[a]		Bias (Percent of Peak SWE)[b]	
SNOTEL ID (Z in m asl)	Observed Peak SWE (mm)		Nonsheltered	Sheltered	Nonsheltered	Sheltered
310 (2782)	2007	145	−5	13	−18.6	−9.7
	2008	305	3	29	8.2	23.0
	2009	254	−18	22	−25.6	−4.7
511 (2750)	2007	218	−21	−10	−26.7	−15.1
	2008	434	−10	10	−7.1	3.9
	2009	243	−19	10	−20.6	−0.4
705 (2418)	2007	290	−5	7	−18.6	−9.0
	2008	480	15	30	37.7	51.0
	2009	488	−6	21	−12.5	5.7
617 (2805)	2007	168	−17	−2	−25.6	−8.3
	2008	417	−9	16	−6.2	6.7
	2009	333	−7	18	−21.3	−1.5
416 (2561)	2007	89	−25	1	−30.3	−15.7
	2008	201	−6	12	−15.4	20.4
	2009	99	−34	−5	−42.4	−34.3
866 (2393)	2007	94	−14	6	−30.4	−9.7
	2008	150	12	32	54.0	84.0
	2009	122	7	29	4.9	45.1
902 (2436)	2007	-[c]	-	-	-	-
	2008	193	−6	7	−12.4	15.0
	2009	114	−35	−11	−39.5	−26.3
519 (2329)	2007	140	−16	−2	−30.0	−20.0
	2008	287	2	15	25.8	48.1
	2009	241	−41	1	−30.3	−5.8
877 (2104)	2007	198	−35	−28	−36.9	−33.3
	2008	193	−7	15	10.4	66.3
	2009	345	−43	−4	−31.6	−17.4

[a]Positive values indicate longer persistence than observed.
[b]Positive values indicate greater simulated SWE than observed. Periods when both SWE values are zero are not considered in bias calculation.
[c]Not considered in water year 2007 as the site displayed ~25 mm (~200%) more SWE than precipitation accumulation by 20 January 2007.

Journal of Geophysical Research: Atmospheres

10.1002/2016JD025184

Table 4. Agreement Measures Between AmeriFlux Observations and Model Input/Simulated Sublimation[a]

	Sublimation/Flux (mm)[b]				T (K)			W (ms^{-1})			RH (%)			P (mm)[c]	
	r	NSE	Simulation[c]	Observation[c]	r	Simulation	Observation	r	Simulation	Observation	r	Simulation	Observation	Simulation	Observation
VMC 2008 ($n = 700$)	0.39	−0.28	74.2	47.0	0.86	269.8	269.5	0.35	4.5	3.6	0.79	55.8	53.0	387	351
VMC 2009 ($n = 512$)	0.37	0.13	58.7	59.8	0.88	272.1	271.4	0.33	4.9	3.4	0.73	52.2	49.9	284	288
VMC 2010 ($n = 553$)	0.13	−0.08	56.5	49.5	0.78	270.3	270.2	0.32	4.2	3.0	0.65	54.4	50.9	391	394
FUF 2007 ($n = 216$)	0.46	0.15	13.3	12.4	0.84	270.5	272.2	0.61	4.8	3.1	0.78	60.4	53.4	61	55
FUF 2008 ($n = 553$)	0.39	−0.02	36.6	36.7	0.85	271.7	272.5	0.58	5.2	2.9	0.77	58.7	56.5	219	172

[a]The half-hourly AmeriFlux data were coarsened to the 3-hourly model time step. If there was any missing observational data in a given time step, the time step was not considered. The number of 3-hourly time steps for the flux data is given by n. The sample size for meteorological variables was commonly higher.
[b]Averages from the high sublimation (HSUB) and low sublimation (LSUB) simulations are displayed.
[c]Summed for all time steps, all other values are averages.

important because unlike the SNOTEL network and other common meteorological networks, precipitation from the AmeriFlux network is not assimilated into the daily PRISM data (http://www.prism.oregonstate.edu/documents/PRISM_datasets.pdf).

Correlations between modeled $SUB_g + SUB_i$ and tower vapor flux range from 0.13 to 0.46 (Table 4) and compare reasonably well to those reported in other subdaily modeling studies. For example, driven by local meteorological observations and with site-specific calibration, *Mahat et al*. [2013] report correlations between simulated and observed above canopy latent heat flux ranging from 0.37 to 0.54 for years 2003–2010 at the Niwot Ridge Forest AmeriFlux site in Colorado, USA. Bias varies from year to year, which is partly responsible for the wide range in Nash-Sutcliffe efficiency (NSE), from −0.28 in 2008 at the VMC site to 0.15 in 2007 at the FUF site (Table 4). The magnitude of bias is comparable to *Broxton et al*. [2014], who simulated above canopy vapor flux at the VMC site using local meteorological observations as input. For the years 2008–2010, *Broxton et al*. [2014] report a consistent positive flux bias, as high as ~20% in 2010.

To further explore agreement with AmeriFlux tower observations, time series of observed vapor flux and modeled sublimation are displayed for FUF in 2007, the highest correlation and NSE in Table 4, and VMC 2010, the lowest correlation in Table 4 (Figures 4 and 5). Mean absolute error (MAE) and bias are highly variable in 2010 at the VMC site, with two periods of poor agreement in late January to early February and mid-March (Figure 4). The large low bias in mid-March appears to be related to a large precipitation-interception event. For periods within 2 days of a snowfall event, observed fluxes at the VMC site in 2010 were 1.32 mm d^{-1} while simulated $SUB_i + SUB_g$ was 0.79 mm d^{-1} (Table 5). Agreement after precipitation is better for other events. For example, low mean absolute error (less than 0.09 mm) is evident for late March, spanning multiple precipitation events (Figure 4).

Bias and MAE appear to be relatively consistent in time at the FUF site in 2007, with MAE less than 0.1 mm spanning several precipitation events (Figure 5). An exception is late February, with daytime temperatures consistently above 7°C since early February, transpiration within the instrumentation footprint may have contributed to higher flux measurements. The snow season positive bias (Table 4) appears to be the result of a consistent slight positive bias, with the exception of periods just after some precipitation events when bias drops to near 0 mm (Figure 5). For periods within 2 days of a snowfall event, observed fluxes at the FUF site in 2007 were 0.47 mm d^{-1} while simulated $SUB_i + SUB_g$ was 0.49 mm d^{-1} (Table 5). It is possible that this is evidence of good agreement between modeled canopy and observed canopy sublimation; however, flux observations beneath the forest canopy are required to isolate the contribution of canopy sublimation from total above canopy fluxes. Unfortunately, subcanopy flux observations are not available at these sites.

Correlations are generally greatest during periods with most recent snowfall longer than 2 days prior and high-wind periods (Table 5). Across both sites, agreement is generally the poorest at night and during periods within 2 days of snowfall, with low correlations and large bias relative to other periods examined (Table 5). In particular, there is a large positive bias (at least 0.2 mm d^{-1}) at night for both sites across all years of simulation (Table 5). Biases tend to be positive for periods with most recent snowfall longer than 2 days prior and negative with large magnitude (as low as −1.17 mm d^{-1}) during periods within 2 days of snowfall (Table 5). Biases are similar (generally $<$0.13 mm d^{-1} in magnitude) between both low-wind and high-wind periods (Table 5).

4.3. Basin-Scale Simulations

The contrast in total snowfall between 2007 and 2008 is greatest at the highest elevations in the eastern portion of the Salt (Figures 1 and 6), with approximately twice the snowfall in 2008 (e.g., ~800 mm in 2008 and 400 mm in 2007). Snowpack sublimation (SUB_g) and canopy sublimation (SUB_i) are displayed for the LSUB simulations in Figure 6. The largest increases in canopy sublimation from LSUB to HSUB simulations (not shown) are at the highest elevations with a maximum increase of 6 mm in 2008 and 8 mm in 2007. Similarly, the largest increases in ground sublimation are at the highest elevations, with a maximum of 13 mm (7 mm) more ground sublimation for the HSUB simulation in 2008 (2007) than LSUB simulations.

Canopy sublimation in 2007 and 2008 are very similar despite the greater snowfall in 2008 (Figure 6), suggesting that large amounts of simulated snowfall were not intercepted by the canopy in 2008. Averaged for both HSUB and LSUB simulations, 11% of the snowfall was intercepted across the entire study area in 2008, compared to 19% in 2007. Likely owing to the large snowfall totals, snowpack sublimation exceeds 100 mm across

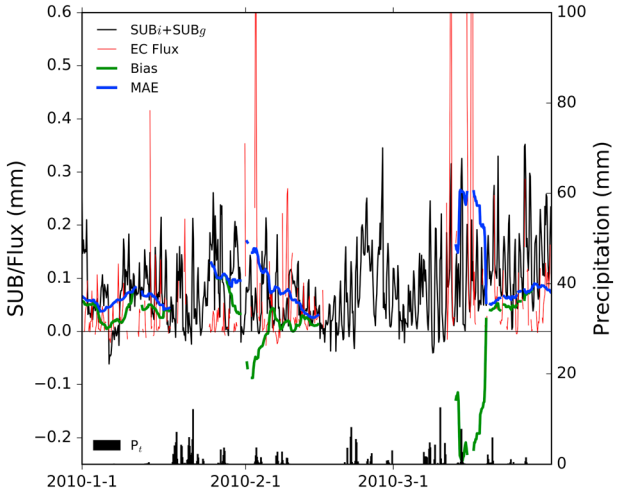

Figure 4. Displayed only for 1 January to 31 March 2010 for visual clarity, precipitation (P_t), simulated total sublimation ($SUB_i + SUB_g$), and eddy-covariance measured vapor flux (EC flux) at the VMC AmeriFlux site. Running bias and MAE are for a 5 day centered sliding window with no more than 50% observational data missing.

much of the high elevation areas in 2008, with a maximum of 191 mm (Figure 6). In contrast, maximum snowpack sublimation is less than 100 mm in 2007 (Figure 6).

4.4. Sensitivity to LAI* Reduction

4.4.1. Radiation and Wind Speed

Upon a 30% LAI* reduction, the maximum increase in subcanopy shortwave flux is more than 0.13 W m^{-2} per unit unadjusted flux (equation (2) and Figure 7). This can be interpreted as an increase of 13 W m^{-2} per 100 W m^{-2} of shortwave flux at the top of the canopy. This maximum occurs at about 1.65 initial LAI* (LAI_o) and drops to ~0.09 W m^{-2} per unit unadjusted flux at 0.69 LAI_o and to ~0.12 W m^{-2} at 2.50 LAI_o (Figure 7). For wind speed in the LSUB simulations (equation (9)), this maximum occurs at about 3.30 LAI_o, which is greater than the maximum LAI* (2.40) in the Salt derived from the 30 m NLCD 2011 and equation (1). The increase in the subcanopy wind speed upon a 30% LAI* reduction therefore decreases monotonically from 2.40 LAI_o to 0.30 LAI_o for both HSUB and LSUB simulations (Figure 7). It is important to note that adjustment to longwave radiation for the subcanopy is a function of the natural log of LAI* (equations (3) and (4)). Thus, the change in longwave radiation due to LAI* reduction does not vary with initial LAI* (LAI_o).

On average across the basin for both 2007 and 2008, wind speed increases by 1.00 m s^{-1} per ~845 m increase in elevation. This suggests that the increase in wind speed upon a 30% reduction in LAI* was on average 0.09 m s^{-1} greater at 2845 m asl than 2000 m asl at 1.20 initial LAI* (LAI_o) for both HSUB and LSUB simulations (Figure 7).

The decrease in longwave radiation upon a 30% LAI* reduction varies little through the snow season, while the increase in absorbed shortwave radiation is substantially greater in the spring than the winter (Figure 8a). For example, averaged for both 2007 and 2008, the difference in absorbed shortwave radiation for 1.51 LAI* and 1.06 LAI* noticeably increases after 1 March for 2200 m asl flat terrain (Figure 8a). This results in a transition from a decrease in total absorbed radiation before March to an increase in late winter and spring (Figure 8 a). This transition is represented by the minimum on curves representing the accumulating change in total absorbed radiation upon a 30% LAI* reduction (Figure 8b).

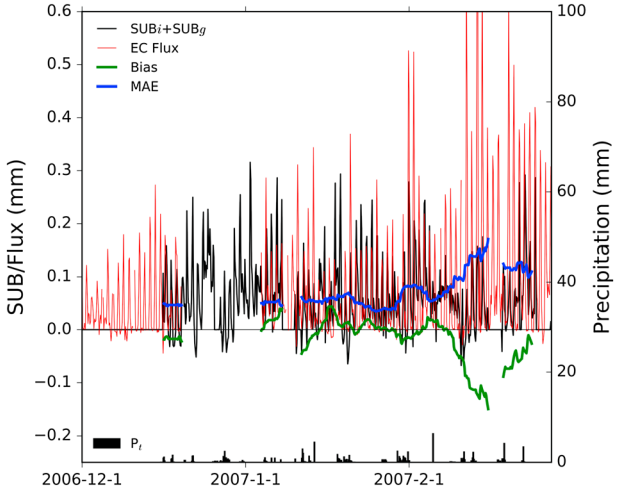

Figure 5. Same as in Figure 4 but for the FUF site in water year 2007.

Gaining elevation, the decrease in incoming longwave radiation from LAI* reduction overcomes the increase in shortwave radiation (not shown). Therefore, the

Journal of Geophysical Research: Atmospheres

10.1002/2016JD025184

Table 5. Agreement Measures Between AmeriFlux Observations and Simulated Sublimation for Six Categories: More Than 2 Days Since the Last Snowfall, Less Than 2 Days Since the Last Snowfall, Incoming Solar Radiation Greater Than 0 W m^{-2}, Incoming Solar Radiation Equal to 0 W m^{-2}, Wind Speed Greater Than or Equal to the Median Speed, and Wind Speed Less Than the Median[a]

	Last SFE, >2 days[b] Sublimation/Flux (mm d^{-1})			Last SFE, ≤2 days Sublimation/Flux (mm d^{-1})			$Q_{si} > 0.0$ W m^{-2} Sublimation/Flux (mm d^{-1})			$Q_{si} = 0.0$ W m^{-2} Sublimation/Flux (mm d^{-1})			High W Sublimation/Flux (mm d^{-1})			Low W Sublimation/Flux (mm d^{-1})		
	r	Simulation	Observation	r	Simulation	Observation	r	Simulation	Observation	r	Simulation	Observation	r	Simulation	Observation	r	Simulation	Observation
VMC 2008	0.53	0.84	0.44	0.18	0.92	0.85	0.36	1.01	0.71	0.23	0.62	0.27	0.39	1.01	0.61	0.37	0.70	0.47
VMC 2009	0.42	0.90	0.68	0.41	1.02	2.19	0.35	1.06	1.29	0.05	0.66	0.31	0.45	1.17	1.13	0.17	0.69	0.76
VMC 2010	0.29	0.80	0.45	0.08	0.79	1.32	0.13	0.87	0.94	−0.04	0.68	0.31	0.21	0.92	0.81	0.06	0.70	0.61
FUF 2007	0.62	0.50	0.45	0.35	0.49	0.47	0.47	0.56	0.71	0.12	0.38	0.06	0.53	0.56	0.44	0.41	0.44	0.49
FUF 2008	0.45	0.59	0.45	0.42	0.39	0.72	0.35	0.65	0.78	0.19	0.33	0.13	0.37	0.71	0.65	0.41	0.41	0.45

[a]The half-hourly AmeriFlux data were coarsened to the 3-hourly model time step. If there was any missing observational data in a given time step, the time step was not considered.
[b]Averages from the high sublimation (HSUB) and low sublimation (LSUB) simulations are displayed.

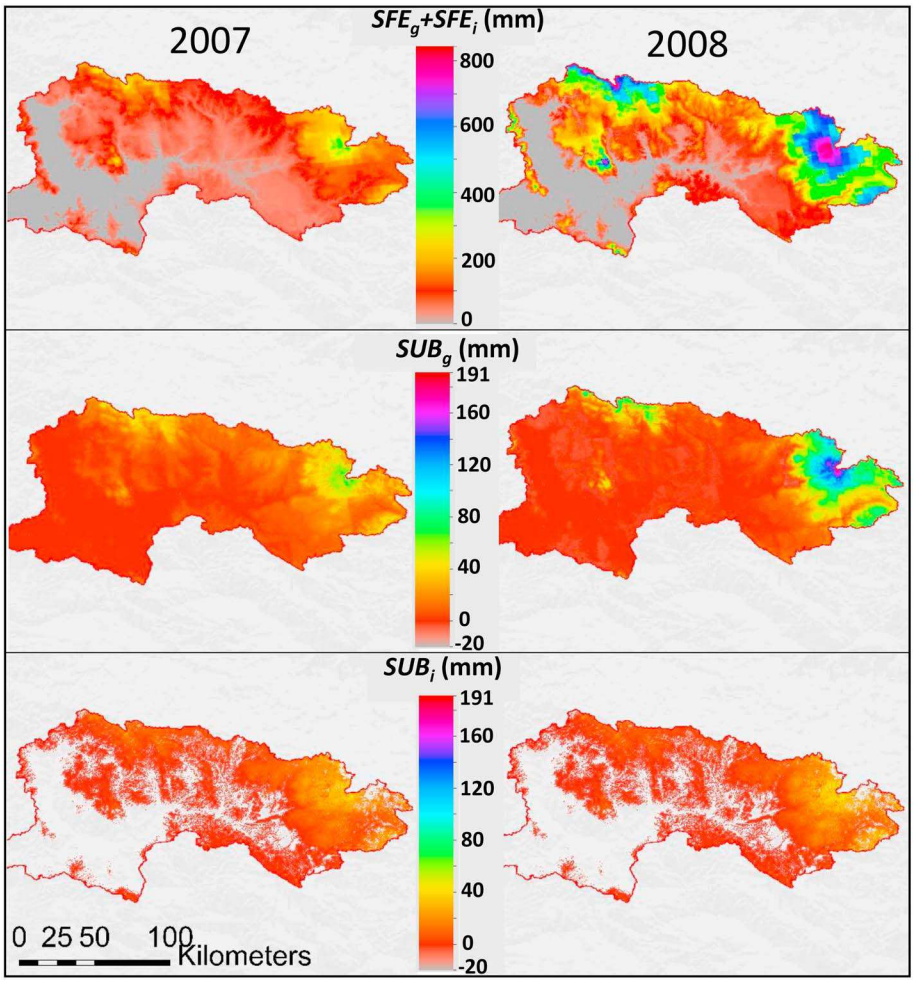

Figure 6. Snow season totals of (top) total snowfall ($SFE_i + SFE_g$), (middle) ground sublimation (SUB_g), and (bottom) canopy sublimation (SUB_i) for the Salt River basin.

decrease upon LAI* reduction in total absorbed radiation during winter is larger at higher elevations (Figure 8 b). The effects of aspect are very apparent (Figure 8b). Averaged for both 2007 and 2008, at an LAI_o of 1.51 (CC = 45%), a 30% reduction in LAI* resulted in 3 times less radiation absorbed by the snowpack by 1 March for north facing 32.5° slopes than south facing 32.5° slopes (Figure 8b). For north aspects, the changes in the longwave radiation budget are much greater than the changes in shortwave radiation. For example, total absorbed radiation does not become consistently greater for reduced LAI* than for full LAI* simulations until April for north aspects with slopes of 32.5° (Figure 8b). In contrast, the increasing solar insolation of late winter results in shortwave budget changes overcoming changes in the longwave budget by 1 March for south aspects (Figure 8b). A south aspect snowpack persisting until 1 April displays little change in absorbed radiation, while a north aspect experiences 70 MJ m^{-2} less absorbed radiation by 1 April upon 30% LAI* reduction (Figure 8b).

4.4.2. Basin Scale

Simulated snowfall below 1250 m asl was minimal. For both years, distributed evenly above 1250 m asl (~12,776 km^2) end of season changes in simulated canopy sublimation ($\sum \Delta SUB_i$) with 30% LAI* reductions range from ~1.05 mm (23.0%) in 2007 to ~1.29 mm (27.0%) in 2008 (Figure 9). Ground sublimation also decreased by ~0.17 mm in 2007 and ~0.72 mm in 2008 (Figure 9). This corresponds to a decrease in forested area ground sublimation of 1.5% in 2007 and 4.75% in 2008. The wet year to dry year difference in the change from reduced LAI* is 125% greater for ground sublimation than canopy sublimation.

The reduction in SUB_i is episodic due to the reduced interception during precipitation events (Figure 9). The seasonal evolution of the change in SUB_g is more complex with three distinct periods of ΔSUB_g. First, ground

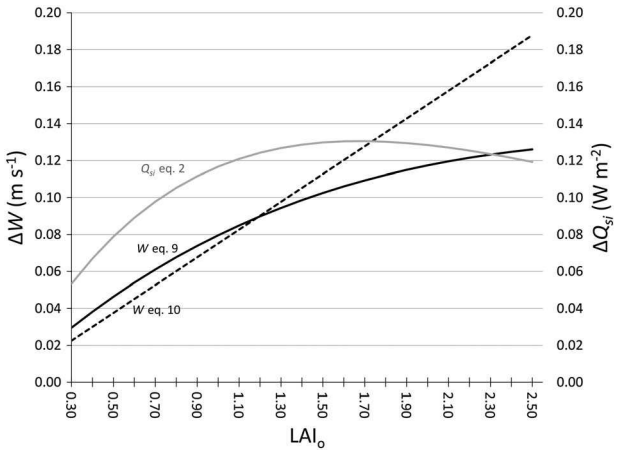

Figure 7. Per unit unadjusted value, the increase in vegetation adjusted wind speed (W) and incoming solar radiation (Q_{si}) over the snowpack upon a 30% LAI^* reduction by initial LAI^* (LAI_o).

sublimation is decreased with LAI^* reduction until early February. Second, SUB_g is increased until early to mid-March. Third, SUB_g generally decreases for the remainder of the season. All three periods of ΔSUB_g are noticeably larger in magnitude at the basin scale in 2008 than 2007 (Figure 9).

Even for south aspects, total absorbed radiation is decreased from LAI^* reduction during winter (Figure 8). The period of decreased snowpack sublimation suggests that the decrease in longwave radiation from reduced LAI^* overcomes the effects increased solar radiation and wind speed during the winter at the basin scale. With increasing solar insolation in late winter, it is likely that the decrease in longwave radiation no longer overcomes the increase in wind speed and shortwave radiation, thereby increasing sublimation with LAI^* reduction. Total absorbed radiation by the snowpack is increased in spring (Figure 8) so the final period of decreased sublimation is potentially due to a decrease in snowpack duration rather than a decrease in sublimation rate.

4.4.3. LAI^* Change and Elevation

In both years, simulated full LAI^* SUB_g is more rapid than reduced LAI^* simulations in December–January (Figures 10a and 10b). In 2007, however, the snowpack was intermittent at 2200 m asl. Specifically, for the flat terrain 1.19 LAI_o simulations shown in Figure 11, the snowpack was absent for 19 days in December–January at 2200 m asl, lessening the cumulative effects relative to the higher elevations (Figures 11a and 11b). Approximately 850 km^2 of land is within 100 m of 2200 m asl. This is considerably greater area than higher elevations, where the snowpack was more continuous in winter. For example, 687 km^2 of land is within 100 m of 2500 m asl and only 188 km^2 within 100 m of 2900 m asl. This leads to a lesser decrease in winter SUB_g upon 30% LAI^* reduction at the basin scale in 2007 than 2008 (Figure 9).

In 2008, the snowpack persists into April and May at 2500 and 2900 m asl. The simulated snowpack at these elevations was exposed to increased radiation and wind speed (Figures 7 and 8) in the reduced LAI^* simulations during spring, resulting in a longer period of increased sublimation rates than the simulations at 2200 m asl (Figures 10 and 11). Despite this long period of increased sublimation rates in 2008 at higher elevations, the total change in SUB_g is negative upon reducing LAI^* (Figure 11b). This is due to a longer duration of the snowpack in the full LAI^* simulations. For example, while the rate of April–May sublimation for the flat terrain simulation at 2900 m asl is greater for reduced LAI^* than full LAI^* (~1.35 mm d^{-1} versus ~1.24 mm d^{-1} in Figure 10b), the snowpack persisted beyond 1 May for only the full LAI^* simulation, resulting in seven more days of sublimation at high rates (Figure 11b). This is further illustrated with plots of SWE in Figure S1 that clearly show increased spring melt rates for reduced LAI^*. For the 2500 m asl simulation, the reduced duration decreases ΔSUB_g by ~7 mm, resulting in a total decrease in SUB_g that is comparable to the decrease in SUB_i (Figure 11b). Thus, the extended duration of the snowpack in 2008 at high elevations contributes not only to large increases in late winter/early spring SUB_g but also to large decreases in spring SUB_g. This is also evident at the basin scale in 2008 (Figure 9).

The greater decrease in SUB_i with elevation displayed in Figure 11 follows from greater snowfall (Figure 6) and thus interception at higher elevations. For example, averaged for the wet and the dry years, snowfall

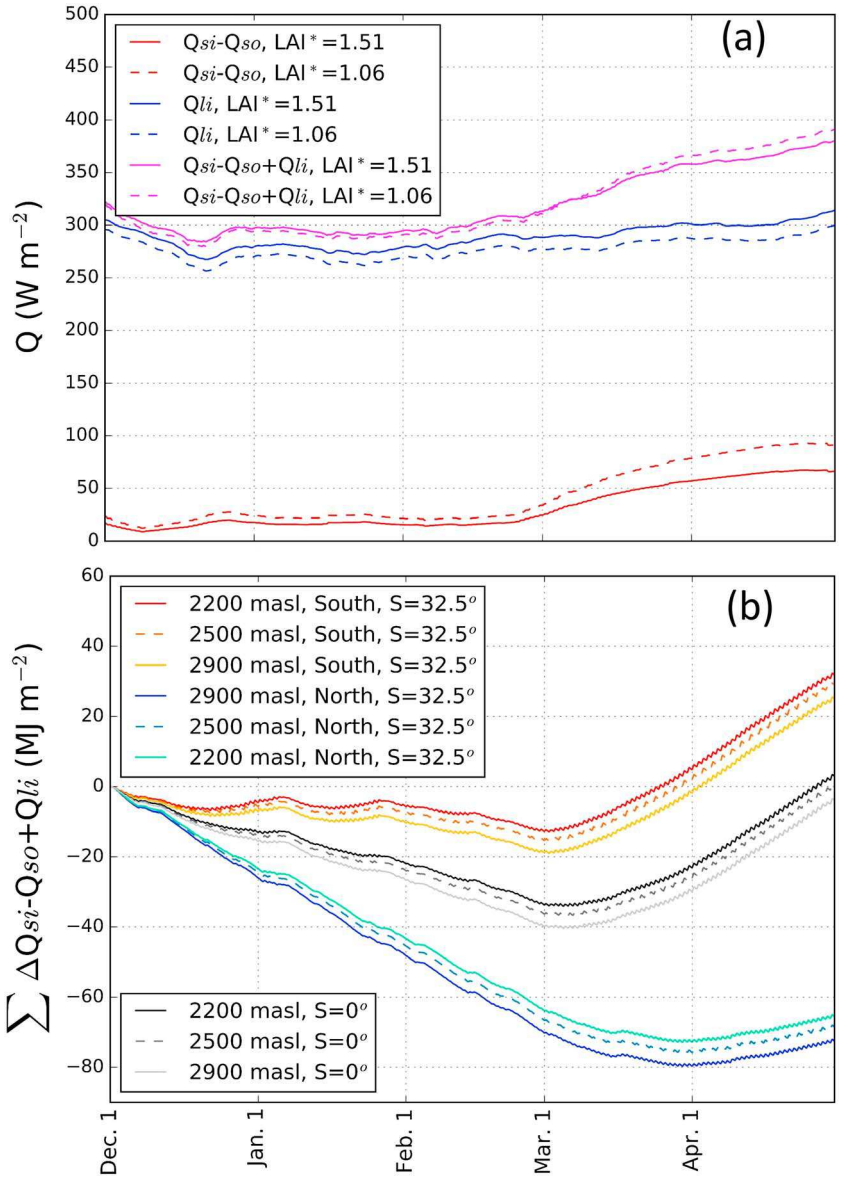

Figure 8. For initial LAI* (LAI_o) 1.51, assuming a snowpack persisting until 30 April, basin-wide averages of (a) incoming longwave radiation (Q_{li}), absorbed shortwave radiation ($Q_{si} - Q_{so}$), and total absorbed radiation ($Q_{si} - Q_{so} + Q_{li}$) for 2200 m asl flat terrain as well as (b) accumulating changes in total absorbed radiation ($Q_{si} - Q_{so} + Q_{li}$) upon 30% LAI* reduction for selected terrain types. The average of 2007 and 2008 is displayed, and the values in Figure 8a are 20 day centered averages for visual clarity.

interception at 1.19 LAI* is 52.6 mm, 63.4 mm, and 73.2 mm at 2200 m asl, 2500 m asl, and 2900 m asl, respectively. Another reason is the decreased percentage of intercepted snow that is unloaded before sublimation. This percentage is 72%, 69%, and 56% in the 2200, 2500, and 2900 m asl simulations, respectively. The higher fractions of unloaded snow at lower elevations are due to increased temperature (equation (7)). The greater decrease in SUB_i at 2500 and 2900 m asl in 2008 than 2007 (Figures 11a and 11b) follows from the greater snowfall in 2008. In particular, average canopy snow storage was greater in 2008 than 2007 by 23% and 18% at 2500 and 2900 m asl, respectively. This is despite the slightly greater frequency of precipitation in 2007 than 2008 (26% versus 21%, respectively). In contrast, the decrease in SUB_i is slightly greater in 2007 than 2008 in the 2200 m asl simulation. Average canopy snow storage was 4% less in 2008 than 2007 at full LAI* despite greater snowfall in 2008. In addition to greater precipitation frequency in 2007, this was due to more frequent unloading in 2008, with 60 more hours of above melting point temperatures during

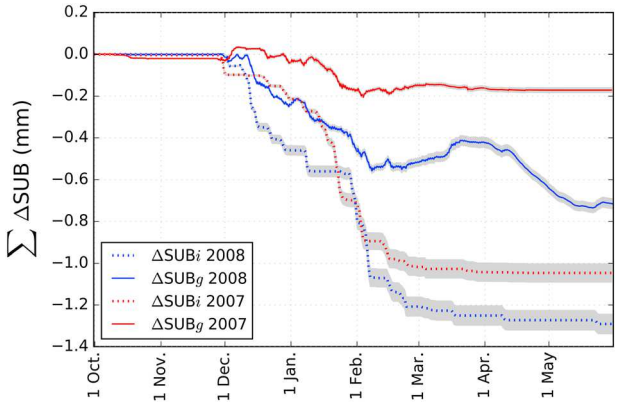

Figure 9. For a 30% LAI* reduction, the accumulating change in sublimation for the Salt River basin given in depth distributed evenly above 1250 m asl, an area of 12,776 km^2. The average of the high sublimation (HSUB) and low sublimation (LSUB) simulations for intercepted sublimation (SUB_i; dotted lines) and ground sublimation (SUB_g; solid line) for 2007 (red lines) and 2008 (blue lines) are displayed. The gray envelopes represent the range of the HSUB and LSUB simulations.

December–March of water year 2008 than 2007 (see equation (7)). This led to 77% of the intercepted snowfall not sublimating in 2008 versus 66% in 2007.

4.4.4. LAI* Change and Initial LAI*

In this section, results from flat terrain simulations at 2500 m asl across a forest cover density gradient are displayed. The patterns discussed below are also found for 2200 and 2900 m asl simulations (not shown) but are clearest at 2500 m asl. Snow cover duration does not appear to be the primary impact on ΔSUB_g with LAI* reduced by 30% across a forest cover density gradient with $LAI_o = 2.47$, 1.51, and 0.87 (Figures 11c and 11d). Rather, the combined effect of changes in radiative input and wind speed (Figures 7 and 8) appear to be of primary importance. For $LAI_o = 0.87$, the increase in shortwave radiation and wind speed is lesser than denser forests (Figure 7), resulting in lesser rates of SUB_g in the winter for reduced LAI* simulations (Figure 10). For $LAI_o = 2.47$, the larger increases in wind speed and shortwave radiation upon 30% LAI* reduction (Figure 7) overcome the decreased longwave radiation (Figure 8), resulting in increased rates of SUB_g in winter upon reduced LAI* (Figures 10c and 10d). In February–March, SUB_g rates are greater for reduced LAI* (Figure 10) for all values of LAI_o (0.87, 1.51, and 2.47) due to increasing solar insolation relative to early winter (Figure 8). The difference in February–March SUB_g rates are greatest for $LAI_o = 2.47$ due to the large increase in both wind speed and shortwave flux upon LAI* reduction.

Snow cover duration (Figures 11c and 11d) accounts for notable differences between the dry year simulation (2007) and the wet year simulation (2008). For example, at 2500 m asl, snow persists nearly 50 days longer into spring in 2008. This extended period of increased SUB_g rate resulted in 4 mm more SUB_g in the reduced LAI* simulations from 1 March until the disappearance of the reduced LAI* snowpack in mid-April for moderate forest cover, $LAI_o = 1.51$ (Figure 11d). However, 7 mm of SUBg occurred in the full LAI* simulation after mid-April, resulting in a 2.5 mm net decrease in SUBg (Figure 11d).

The greater decrease in SUB_i within greater LAI_o (Figures 11c and 11d) follows from greater interception. Averaged for both years, simulated intercepted snowfall was 54 mm, 72 mm, and 91 mm for LAI* equal to 0.87, 1.51, and 2.47, respectively. This leads to higher rates of SUB_i with increasing LAI* (Figures 10c and 10d). At 2500 m asl, 335 mm more snowfall liquid equivalent (SFE) occurred in the 2008 than the 2007 simulation. Due to the greater canopy snow-holding capacity in heavily forested areas, this resulted in 39 mm more intercepted snow at LAI* = 2.47 in 2008 than 2007. This contrasts with only 24 mm and 14 mm more intercepted snow in 2008 than 2007 for LAI* = 1.51 and LAI* = 0.87, respectively. Therefore, the decrease in SUB_i upon reduced LAI* is substantially larger in 2008 (~11 mm) than 2007 (~7 mm) for $LAI_o = 2.47$.

4.4.5. LAI* Change and Aspect

In this section, results from $LAI_o = 1.51$ simulations at 2900 m asl for north and south aspect slopes are displayed. The patterns discussed below are also found for lower elevations (not shown) but are clearest at 2900 m asl. The change in radiative input by aspect to the ground snowpack (Figure 8) is important to ΔSUB_g. The relatively small increases in shortwave radiation on north aspects upon LAI* reduction are overcome by the decreases in longwave radiation (Figure 8), resulting in the early period of negative ΔSUB_g lasting until 1 March (Figures 11e and 11f). In contrast, the larger increase in shortwave radiation on south aspects nearly overcomes the decrease in longwave input in winter upon LAI* reduction (Figure 8). When combined with the increased wind speed (Figure 7), ΔSUB_g is slightly positive during the winter (Figures 11e and 11f).

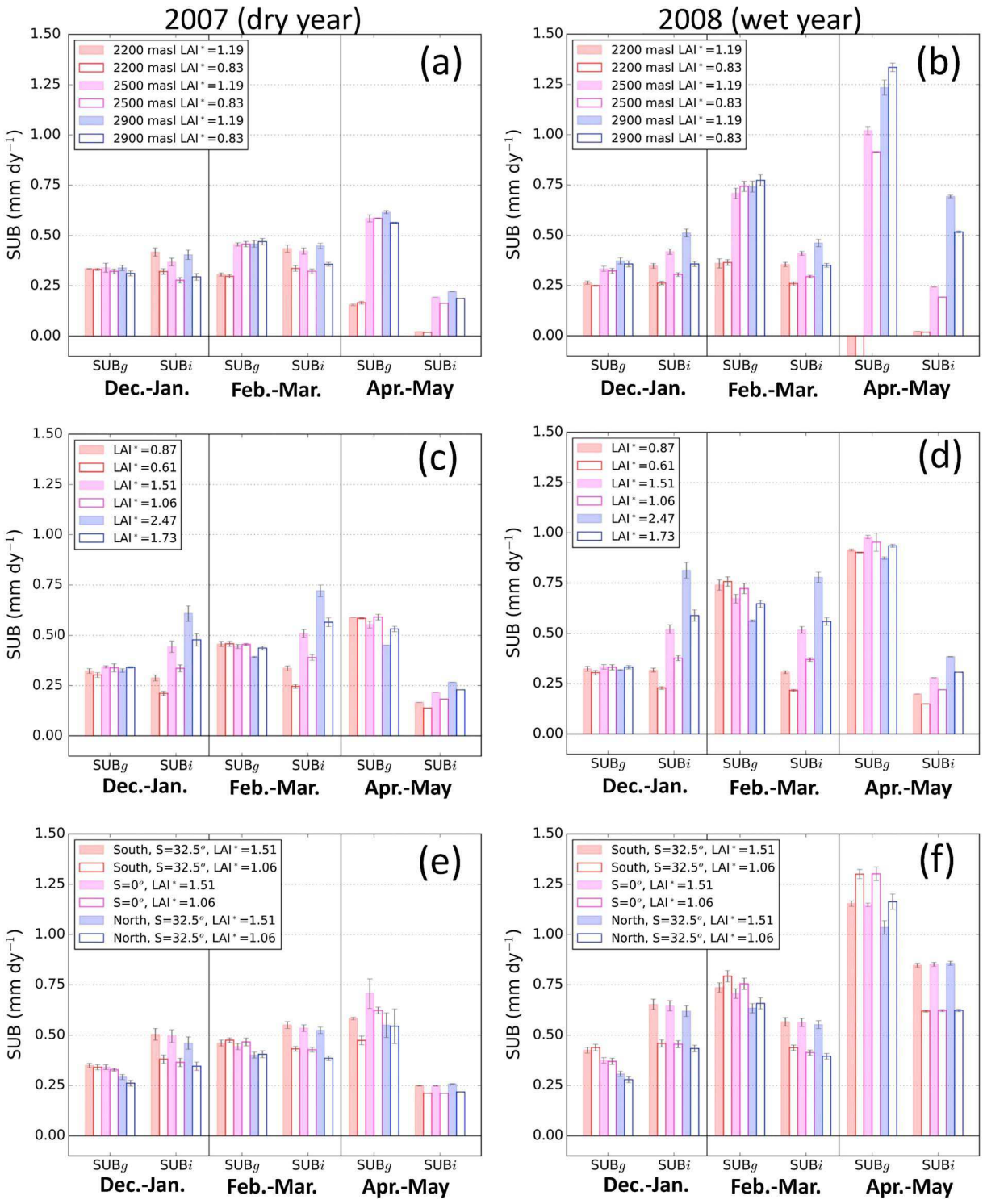

Figure 10. For (a, c, and e) 2007 and (b, d, and f) 2008, the rates of canopy sublimation (SUB_i) and ground sublimation (SUB_g) corresponding to the simulation results displayed in Figure 11. Rates are averaged for each 2 month period with periods without snow cover excluded and averaged for the HSUB and LSUB simulations. Simulations are for flat terrain across an elevation gradient (Figures 10a and 10b), for 2500 m asl and flat terrain across an initial LAI^* (LAI_o) gradient (Figures 10c and 10d), and for 2900 m asl across a slope/aspect gradient (Figures 10e and 10f). The error bars represent the range of the HSUB and LSUB simulations. The locations of the simulations are displayed in Figure 1.

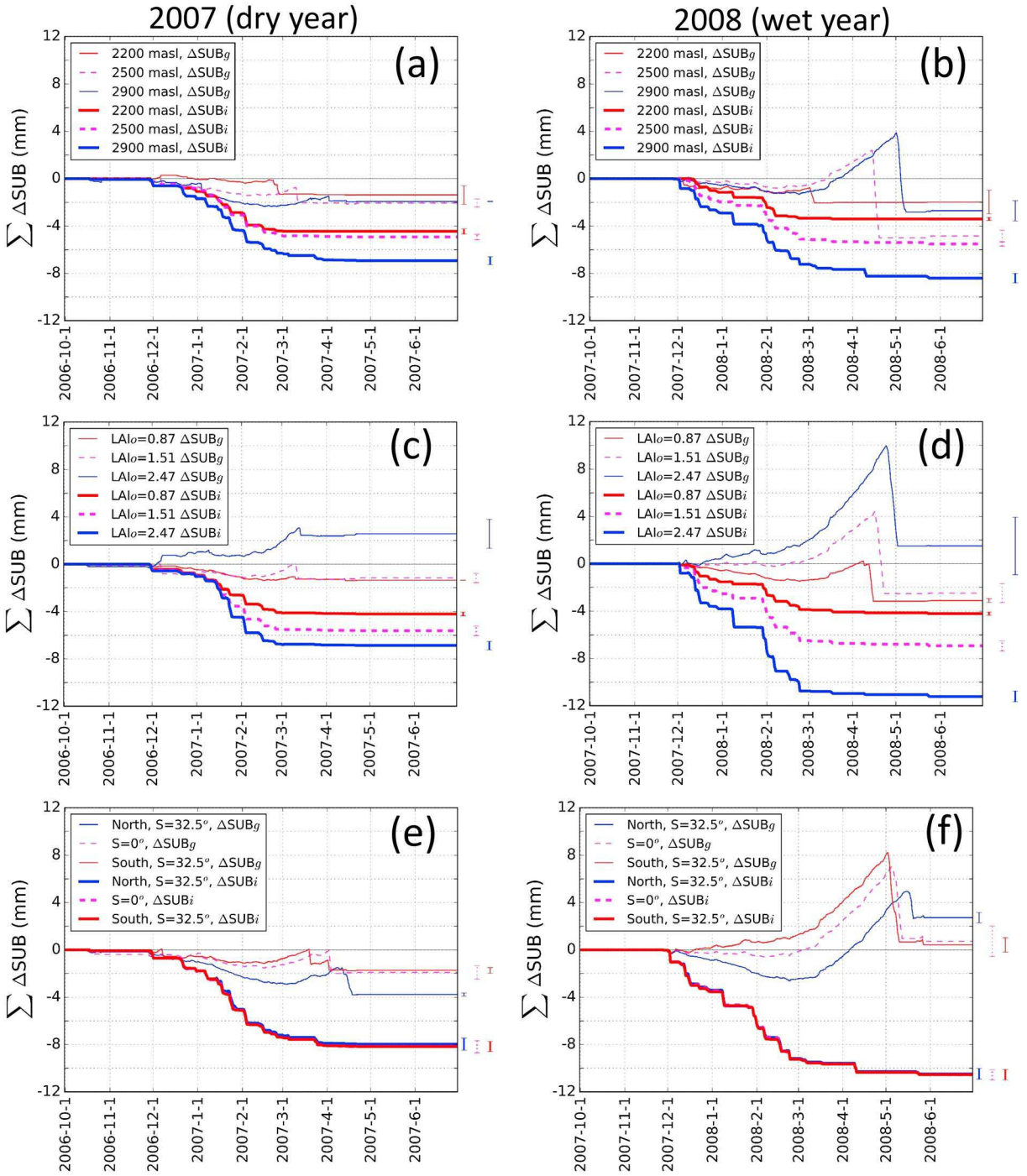

Figure 11. For (a, c, and e) 2007 and (b, d, and f) 2008, accumulating change in canopy sublimation (SUB_i; thick lines) and ground sublimation (SUB_g; thin lines) upon a 30% LAI^* reduction are averaged for the LSUB and HSUB simulations. Simulations are for 1.19 initial LAI^* (LAI_o) and flat terrain across an elevation gradient (Figures 11a and 11b), 2500 m asl flat terrain across a forest density gradient (Figures 11c and 11d), and 2900 m asl at 1.51 LAI_o across a slope/aspect gradient (Figures 11e and 11f). The error bars represent the range of the HSUB and LSUB simulations at the end of the season. The locations of the simulations are displayed in Figure 1.

Differences in snow cover duration lead to obvious differences in ΔSUB_g between 2007 and 2008. For example, north aspect total ΔSUB_g by 1 March first is nearly identical for both years, ~−2.5 mm (Figures 11e and 11f). However, the long spring duration in 2008 increases SUB_g by nearly 8 mm from 1 March to mid-May, resulting in an overall increase in SUB_g (Figures 11e and 11f). A similar pattern is evident for south aspects and flat terrain, where total ΔSUB_g is negative in 2007 and positive in 2008.

4.4.6. Interaction Effects of Forest Density, Aspect, and Elevation

Periods of positive ΔSUB_g upon LAI^* reduction are extended by increased elevation and by increased snowfall, which both extend snowpack duration in the spring (Figure 11b). For heavily forested areas ($LAI_o = 2.47$), the increase in wind speed upon 30% LAI^* reduction is greater than areas of lighter forest cover and the increase in shortwave radiation is only slightly less than the maximum at $LAI_o = 1.65$ (Figure 7). Furthermore, the increase in shortwave radiation upon LAI^* reduction is greater for south aspects than flat terrain or north aspects (Figure 8). For wet year (2008) simulations at 3300 m asl, 2.47 LAI_o, 62.5° slope, and a south aspect, total SUB_g is increased by 22.0 mm (Figure S2). This overcomes a 19.5 mm decrease in SUB_i for a total increase in sublimation by 2.5 mm upon 30% LAI^* reduction. This contrasts sharply with the dry year (2007) simulations, where $\Delta SUB_i = -13.5$ mm and $\Delta SUB_g = +3$ mm (Figure S2).

5. Discussion

5.1. Comparisons with Previous Investigations

The change in SUB_g with LAI^* reduction appears to be fundamentally controlled by three interdependent factors: (1) the competing effects of increased wind speed and decreased radiative input in winter, primarily controlled by aspect and initial LAI^* (LAI_o); (2) the duration of snowpack in spring, primarily controlled by elevation and total snowfall (i.e., wet year/dry year); and (3) the change in spring snowpack duration with LAI^* reduction and the meteorological conditions spanning that change. The importance of wet year/dry year differences in duration may be exaggerated in warmer climates such as the Southwest U.S., where snow only persists long into spring at the highest elevations in dry years.

The total change in SUB_i with LAI^* reduction is primarily controlled by the amount of canopy sublimation at LAI_o. More interception occurs with increasing snowfall, but it is limited by the snow-holding capacity [*Boon*, 2012], resulting in similar totals of canopy sublimation, between the wet year (2008) and dry year (2007), relative to the differences in SUB_g (Figure 6). Colder temperatures promote longer canopy snow storage, with 72% of the intercepted snowfall unloading, rather than sublimating in the canopy, at 2200 m asl and only 56% unloading at 2900 m asl.

Several results in this study conflict with the modeling results of previous investigators. For example, in higher-latitude and more humid climates, *Strasser et al*. [2011] and *Gelfan et al*. [2004] find greater variability in canopy sublimation by wet and dry years than ground sublimation. There are three likely reasons for these discrepancies. First, higher values of LAI^* characterized the forests, 3.4 for *Gelfan et al*. [2004] and as high as 14.0 for *Strasser et al*. [2011]. The maximum LAI^* considered in this study was 2.47. *McDowell et al*. [2008] measure LAI^* in a ponderosa pine stand in New Mexico to be 2.38 ± 0.23 and note that the density of the stand is near the highest observed for ponderosa pine forest in the Southwest U.S. Increasing LAI^* lessens the limiting effects of snow-holding capacity on canopy sublimation. Second, the higher-latitude climates are colder, allowing snow to be stored in the canopy longer. Simulations in this study suggest that only 18% of intercepted snow sublimates in the canopy at lower elevations (e.g., 2200 m asl) due to a high frequency of temperatures above the melting point in winter. Third, with more humid and generally low-energy conditions compared to the southwestern U.S., one would expect rates of ground sublimation to be low compared to rates sublimation from snow in the canopy that has a high surface area to mass ratio.

The high totals of ground sublimation in 2008, particularly at high elevations (Figure 6), are the result of long duration in the spring and high sublimation rates compared to winter (Figures 10 and 11). This contrasts with *Hood et al*. [1999], who find lower sublimation rates in the spring (~0.25 mm d^{-1} in April) than winter, with net deposition in May at an alpine site in front range of the Rocky Mountains in Colorado. The low spring sublimation rates in Colorado reported by *Hood et al*. [1999] could be unique to alpine sites, as *Sexstone et al*. [2016] reported higher sublimation rates (~0.4 to ~0.8 mm d^{-1}) during snowmelt at subalpine sites in central Colorado. In contrast to central Colorado, central Arizona is notably dry in April, May, and June [*Sheppard et al*., 2002], and one would expect the remaining snowpack to be exposed to high-energy and dry conditions that promote high rates of snowpack sublimation (>1.00 mm d^{-1} in Figure 10). *Mahmood and Vivoni* [2014] note the importance of snow cover duration on sublimation for a catchment at a similar latitude to the Salt in New Mexico (35°53′N, 106°17′W).

Ground sublimation in arid regions with high solar elevation angles and many cloud-free days should be sensitive to increased shortwave radiation upon LAI* reduction [*Harpold et al*., 2014]. In Valles Caldera National Preserve in New Mexico, using peak SWE to winter precipitation ratio as a proxy for sublimation, *Harpold et al*. [2014] found increased winter sublimation upon canopy removal by fire. This is not necessarily in contrast to the results in this study as increased SUB_g upon LAI* reduction is clearly evident after 1 March (Figure 11) in this low-latitude study area, particularly for heavily forested and south facing slopes. Changes in longwave radiation from LAI* reduction overcoming changes in shortwave radiation, the "radiative paradox," is most likely to occur during conditions of lower solar elevation angle, high snow albedos, and low atmospheric emissivities [*Lundquist et al*., 2013; *Meromy et al*., 2015]. One would expect these conditions to be common primarily in the winter in the Southwest U.S. and for north aspects (Figures 11e and 11f) as the angle of incident radiation is less than other aspects. Previous studies have noted the "radiative in paradox" for melt rates [e.g., *Sicart et al*., 2004; *Lawler and Link*, 2011]. *Reba et al*. [2012] found that EC-measured sublimation rates in winter were higher at an exposed site than a subcanopy site; however, the contrast in average wind speed between the two sites was larger (~3.6 m s^{-1}) than simulated in this study. For high unadjusted wind speeds of 10 m s^{-1}, at 1.20 LAI*, equations (9) and (10) produce only a 0.9 m s^{-1} decrease in subcanopy wind speeds upon 30% LAI* reduction. In addition to the changes in the radiation budget, one would expect the sign of ΔSUB_g in winter to be sensitive to the changes in wind speed. Correlations between simulated and observed wind speeds were the lowest of the meteorological variables examined (Table 4).

Over a large forested area in Canada, *Schmidt and Troendle* [1992] found an annual canopy sublimation total of about 46 mm. In Oregon, USA, *Storck et al*. [2002] report approximately 100 mm of intercepted snow sublimation. These values are more than simulated over most of the Salt (Figure 6) in this study. One would expect the relative contribution of canopy sublimation to the snow water budget to be dependent on the duration of snow storage in the canopy. This may be unique to warmer and drier climates with low snowfall frequencies and frequent melt unloading in the winter to limit canopy sublimation. Cold regions have nearly continuous snow storage in the canopy during winter [*Yamazaki et al*., 2007] as do snowy temperate regions [*Suzuki and Nakai*, 2008], which contrasts with dry and temperate regions where canopy snow storage is often intermittent. Change in SUB_i upon LAI* reduction relative to total snowfall is low on the basin as whole (0.6% and 1.3% decrease for a 30% LAI* reduction for 2008 and 2007 simulations, respectively). While this percentage is greater in more localized portions of the watershed (e.g., as high as 5%), it is possible that this change in SUB_i would be substantially greater in colder areas than the Salt, where melt unloading in winter is not as common.

Molotch et al. [2007] report average (maximum) EC-measured canopy sublimation rates from 1 March to 10 April 2002 of 0.71 mm d^{-1} (3.7 mm d^{-1}) with 34.8 mm of total SFE at the Niwot Ridge AmeriFlux site in Colorado (40°1′58″N, 105°32′47″W). This site in Colorado is 3050 m asl with average LAI* of 4.2 and a gap fraction of 17%. For the 2900 m asl simulations presented here (Figures 10 and 11), increasing LAI* to 3.49 (i.e., 4.3×0.83) results in an average SUB_i rate of 0.90 mm d^{-1} with a maximum rate of 4.2 mm d^{-1} from 1 March to 10 April 2008. During this period, 31.0 mm of SFE was simulated. One would expect the slightly higher rates simulated in this study than Niwot Ridge in Colorado due to the lower latitude and higher solar insolation.

5.2. Validation with EC and SNOTEL Measurements

It is important to note that close agreement should not always be expected between sublimation simulated here and flux observations at the AmeriFlux towers. For example, the dynamic flux tower footprint is dependent on wind direction, atmospheric stability, and the characteristics of the upwind terrain [*Sogachev et al*., 2004]. Additionally, the presence of liquid water in the flux footprint (e.g., during mixed precipitation events) and transpiration (possible during warm periods in spring) would increase the measured flux values only. The poorer agreement during periods with recent snowfall (Table 5) is understandable, considering that interception in the model is related to LAI* at 30 m resolution, which is a very simple representation of the forest around the AmeriFlux towers. In addition, in complex terrain, the homogeneity assumption of the flux footprint for EC measurement is questionable [*Foken and Wichura*, 1996; *Mahat et al*., 2013]. Lastly, it is possible that the overestimation of sublimation during periods of low solar radiation is partly due to the challenges of using EC as a measurement technique during periods of stable nocturnal conditions [*Mahat et al*., 2013;

Sexstone et al., 2016]. As with this study (Table 5), *Marks et al*. [2008] noted an improved agreement between modeled and EC-measured fluxes when nocturnal periods are excluded.

Comparisons with SNOTEL observations suggest that snowpack duration was underestimated in 2007 and overestimated in 2008 due to the low bias in SWE in 2007 and high bias in 2008 (Table 3). The bias in rain/snow fraction leading to snowfall overestimation in 2008 at the four lowest elevation SNOTEL sites (705, 877, 866, and 519) resulted in the spring snowpack duration difference between 2007 (dry year) and 2008 (wet year) being largely overestimated. For example, for the simulation results displayed in Table 3, the median overestimation of the duration difference between 2007 and 2008 at the four lowest elevation sites was 24 days. This median decreases to 13 days for the four highest elevation sites, and the overestimation is as low as 8 days (Table 3) at the highest SNOTEL site (617). The median of the observed difference in 2008 versus 2007 spring duration at all sites was 13 days. Therefore, the specific values of the differences in ΔSUB_g with LAI^* reduction (e.g., Figures 9 and 11) are likely exaggerated in the simulations for this specific wet year/dry year pair, especially for the lower elevations, and should be taken with caution.

5.3. Range in the HSUB and LSUB Simulations

As seen in Figure 10, the range in rates between the LSUB and HSUB is at most 0.08 mm d^{-1} SUB_i and 0.16 mm d^{-1} for SUB_g. Owing to the large dependence of SUB_i rate on intercepted snow load (equation (5)), the range between HSUB and LSUB simulations generally only overlap when LAI^* is held constant across the slope/aspect gradient (Figures 10e and 10f). The range between HSUB and LSUB simulations suggests more uncertainty in the effects of LAI^* reduction on SUB_g than SUB_i. Although the average of HSUB and LSUB simulations suggest a December–January decrease in SUB_g for all but heavily forested south aspects, the range in the HSUB and LSUB rates generally overlap (Figure 10). There is less overlap in the range of the HSUB and LSUB simulations between reduced LAI^* and full LAI^* simulations for February–March rates (Figure 10). Owing to the larger sample size for calculating average rates in April–May 2008 than 2007, there is a larger range in the LSUB to HSUB rates for SUB_g in 2007 (as large as 0.16 mm d^{-1} in 2007 in Figure 10e) than 2008.

The snow season cumulative effect of the HSUB to LSUB differences in rates generally lead to a 0.8 mm range in total SUB_i change and a 1.5 mm range in total SUB_g change (Figure 11). The ranges in SUB_i are generally 10% of the total change in SUB_i, and the ranges only overlap for the slope/aspect gradient (Figures 11e and 11f). The largest range in accumulated change is nearly 5 mm for SUB_g in 2008 with $LAI_o = 2.47$ for 2500 m asl flat terrain (Figure 11d). Therefore, the specific values of sublimation change reported in this study should be interpreted with caution. However, the key findings in Figure 11 are generally robust to the different parameterizations of unloading and subcanopy wind speed considered here. For example, due to the extended duration of spring snowpack in the wet year 2008, total ΔSUB_g upon LAI^* reduction is generally positive at 2900 m asl in 2008 and negative in 2007 (Figures 11e and 11f). For most of the basin (Figure 9), the combined effects of reduced SUB_g in winter and reduced SUB_g from reduced duration in late-winter early spring results in a total decrease in SUB_g for HSUB and LSUB simulations. This is most evident for the wet year (Figure 9) and for flat terrain with moderate to light forest cover density, especially at 2200 and 2500 m asl (Figure 11).

5.4. Limitations

It is possible that a larger range in simulation results would occur with different model parameterizations and representations of interception, unloading, latent heat fluxes, etc. For example, changing the constants in equations (2)–(4) for longwave and shortwave radiations would alter the curves in Figures 7 and 8. A more aggressive depletion in solar radiation with increased LAI^* might enable changes in the shortwave radiation budget in winter to overcome changes in the longwave radiation budget upon LAI^* reduction. Also, considering the thermal inertia of the canopy [*Gouttevin et al*., 2015] and various representations of snow albedo would also affect the changes in subcanopy snowpack energy budget due to LAI^* reduction.

In addition, the equation for SUB_g (equation (6)) used here assumes stable stratification and medium roughness. If stability adjustments were made for ground snowpack fluxes [e.g., *Koivusalo et al*., 2001] one might expect sublimation rates during period of high solar insolation to increase. *Mahat et al*. [2013] considered roughness length as a tunable parameter and found better agreement with EC flux observations upon

increasing roughness lengths in a subcanopy environment (0.1 m), relative to typical values in open areas (0.01 m). Similar results were found by *Reba et al*. [2014]. *Mahat et al*. [2013] found that simulated snowpack latent heat flux decreased by 55% when roughness length was changed from 0.1 m to 0.01. *Mahat et al*. [2013] note that these results suggest increased turbulence in the subcanopy environment. It is therefore possible that SUB_g was underestimated here in heavily forested areas, but *Mahat et al*. [2013] also question the below-canopy EC flux measurements, as many assumptions for the EC method may not be valid in subcanopy environments.

In addition, alternative representations of canopy interception processes [e.g., *Ellis et al*., 2010; *Moeser et al*., 2016] would most likely have resulted in a greater range in SUB_i than given here because only unloading processes varied between the HSUB and LSUB simulations. Methods producing greater interception than the *Hedstrom and Pomeroy* [1998] snowfall interception model used here would likely result in greater decreases in SUB_i upon LAI^* reduction than displayed in this study.

Also, canopy snow energy balance models that are coupled to the energy budget of the snowpack [e.g., *Mahat et al*., 2013] differ fundamentally from the ice-sphere sublimation model used here that is only coupled to the ground snowpack through unloading. In *Mahat et al*. [2013], sublimation is calculated from vapor pressure deficit by tracking the intercepted snow surface temperature (using basic turbulent energy flux equations) and with meltwater drip resulting when the intercepted snow surface is at the melting point with extra energy available for melting. Also, the intercepted snow surface temperature and the snowpack surface temperature are related through the simultaneous energy balance equations for the snowpack and the canopy snow [*Mahat et al*., 2013].

Given the large number of possible combinations of parameter/model representations, *Essery* [2015] developed a factorial snowpack model system to help quantify uncertainty. With two levels of representation for five snowpack processes, 2^5 model configurations can be employed. Future work should consider a larger number of possible model setups in an attempt to better estimate uncertainty in sublimation sensitivity to forest cover reduction.

There are also several notable factors neglected from the modeling system used here. Reflected shortwave, emitted longwave, and shading from adjacent terrain are neglected, as well as snow redistribution by wind and gravity. Small-scale studies have found wind redistribution of snow to be important to the snow water budget [*Mahmood and Vivoni*, 2014; *Broxton et al*., 2014]. Additionally, temperature inversions arising from local topography are represented at 4 km (not 30 m), the resolution of the PRISM data. Similarly, the PRISM data likely capture some orographic effects on total snowfall, but there are no adjustments for precipitation based on aspect, slope, and wind direction. Thus, simulated snow interception varies little by aspect in these simulations, resulting little variation by aspect in the decreases in SUB_i upon LAI^* reduction (Figures 11e and 11f). Lastly, mixed-conifer forests typically have higher LAI^* than ponderosa pine forests [*McDowell et al*., 2008]. More explicitly differentiating between mixed-conifer and ponderosa pine forests may have increased simulated canopy sublimation at the higher elevations of the watershed.

While this study focused on a single pair of wet and dry years, results may vary within sets of wet years and dry years based on precipitation frequency differences. A dry year with frequent but light snowfall may have a very high portion of snowfall intercepted by the canopy. In contrast, a wet year characterized by only several intense snowfall events might have a low portion of snowfall intercepted. In addition, there may be considerable interannual variability due to the timing of stable snowpack establishment. A deep snowpack that is established in late fall might amplify the effects of canopy cover reduction through the winter.

6. Summary and Conclusions

For a wet year (2008) and dry year (2007), 30 m terrain and forest cover information was used to downscale meteorological data for input into a snow model system to determine the effects of forest cover on snow sublimation from a large mountainous watershed in the Southwest U.S., the Salt River basin. Detailed analyses of changes in radiation, wind speed, canopy sublimation, and ground sublimation upon forest cover reduction were performed. Corresponding to the hypotheses stated in section 1, results suggest that (1) decreasing forest cover decreases ground sublimation at all but the highest elevations of the watershed; (2) at the basin scale, the effects of forest cover change on ground sublimation are notably greater in the wet year than

the dry year due to a more persistent snowpack; and (3) in contrast, the effect on canopy sublimation (a decrease with reduced forest cover) is more similar between the wet and dry years at the basin scale compared to the effect on snowpack sublimation.

Increased forest cover tends to slightly increase ground sublimation in the winter, most prominent for north facing slopes and areas with light forest cover density (e.g., an effective leaf area index of 0.87). In the late winter and spring, increased forest cover greatly reduces the rates of ground sublimation, most prominent on south facing slopes and areas with heavy forest cover density (an effective leaf area index of 2.47). Canopy sublimation increases greatly, moving from lightly forested to densely forested areas due to greater interception. Canopy sublimation increases with increasing snowfall, but the increase is limited due to the canopy snow-holding capacity. In addition, areas with colder temperatures (e.g., higher elevations) that reduce the frequency of melt-unloading events tend to have higher totals of canopy sublimation. This also contributes to greater changes in canopy sublimation upon forest cover reduction.

It is important to note that that there was evidence in the 2008 simulations for increased ground sublimation upon LAI^* reduction. These simulations tended to be for heavily forested midelevation areas (2500 m asl) and moderately to heavily forested high elevations (e.g., $>$2900 m asl), suggesting that increasing wind speed and solar radiation to a snowpack already persisting long into spring overcomes the effects of shorter duration. For example, in 2008, it was found that steep, heavily forested, and south facing slopes at the highest elevations have increases in ground sublimation upon forest cover reduction that are greater magnitude than decreases in canopy sublimation. In contrast, in the 2007 simulations, the effects of shorter duration in spring tended to overcome the higher-energy conditions resulting from forest cover reduction, even for high elevation, south facing, heavily forested slopes.

Despite the model uncertainties, the results in this study are promising from a water resource perspective. Considering the good agreement with vapor flux, meteorological, and SWE observations shown here, it may be possible to identify key areas of a large watershed that are most sensitive to forest cover change if a model intercomparison approach that focuses on altering more parameterizations is used. This is made more important considering recent trends toward a drier climate in central Arizona and the southwestern U.S. [*Svoma et al*., 2010] that are expected to continue this century [*Seager et al*., 2007; *Ellis et al*., 2008].

Acknowledgments
The model code, model output, and supporting data for all figures and tables will be made available by the author (Bohumil M. Svoma: svomab@-missouri.edu) upon request. This work has been funded by the Salt River Project Agricultural Improvement and Power District grant 13084952 and the University of Missouri Research Board grant 3761 and partially funded by the National Science Foundation under award 1355406, *The Missouri Transect*: *Climate*, *Plants*, *and Community*.

References

Adams, H. D., and T. E. Kolb (2004), Drought responses of conifers in ecotone forests of northern Arizona: Tree ring growth and leaf $\delta^{13}C$, *Oecologia*, *140*, 217–225.

Arya, S. P. (2001), *Introduction to Micrometeorology*, 2nd ed., pp. 79, Academic Press, San Diego, Calif.

Aubinet, M., et al. (2000), Estimates of the annual net carbon and water exchange of forests: The EUROFLUX methodology, *Adv. Ecol. Res.*, *30*, 113–175.

Baker, L. A., T. M. Qureshi, and M. M. Wyman (1998), Sources and mobility of arsenic in the Salt River watershed, Arizona, *Water Resour. Res.*, *34*(6), 1543–1552, doi:10.1029/98WR00627.

Barnett, T. P., J. C. Adam, and D. P. Lettenmaier (2005), Potential impacts of a warming climate on water availability in snow-dominated regions, *Nature*, *438*(7066), 303–309, doi:10.1038/nature04141.

Bernhardt, M., K. Schulz, G. E. Liston, and G. Zängl (2012), The influence of lateral snow redistribution processes on snow melt and sublimation in alpine regions, *J. Hydrol.*, *424–425*, 196–206, doi:10.1016/j.jhydrol.2012.01.001.

Biederman, J. A., et al. (2014), Multiscale observations of snow accumulation and peak snowpack following widespread, insect-induced lodgepole pine mortality, *Ecohydrology*, *7*, 150–162.

Bolin, B., M. Seetharam, and B. Pompeii (2010), Water resources, climate change, and urban vulnerability: A case study of phoenix, Arizona, *Local Environ.*, *15*(3), 261–279, doi:10.1080/13549830903575604.

Boon, S. (2012), Snow accumulation following forest disturbance, *Ecohydrology*, *5*, 279–285.

Brock, B. W., and N. S. Arnold (2000), A spreadsheet-based (Microsoft Excel) point surface energy balance model for glacier and snow melt studies, *Earth Surf. Processes Landforms*, *25*(6), 649–658.

Broxton, P. D., A. A. Harpold, J. A. Biederman, P. A. Troch, N. P. Molotch, and P. D. Brooks (2014), Quantifying the effects of vegetation structure on snow accumulation and ablation in mixed-conifer forests, *Ecohydrology*, *8*, 1073–1094.

Cooper, D. J. (1987), Abert's squirrel above treeline on the San Francisco Peaks, Arizona, *Southwestern Nat.*, *32*, 507.

Daly, C., M. Halbleib, J. I. Smith, W. P. Gibson, M. K. Doggett, G. H. Taylor, J. Curtis, and P. P. Pasteris (2008), Physiographically sensitive mapping of climatological temperature and precipitation across the conterminous United States, *Int. J. Climatol.*, *28*(15), 2031–2064.

Déry, S. J., and M. K. Yau (2002), Large-scale mass balance effects of blowing snow and surface sublimation, *J. Geophys. Res.*, *107*(23), 4679, doi:10.1029/2001JD001251.

Dore, S., T. E. Kolb, M. Montes-Helu, B. W. Sullivan, W. D. Winslow, S. C. Hart, J. P. Kaye, G. W. Koch, and B. A. Hungate (2008), Long-term impact of a stand-replacing fire on ecosystem CO_2 exchange of a ponderosa pine forest, *Global Change Biol.*, *14*(8), 1801–1820.

Dore, S., T. E. Kolb, M. Montes-Helu, S. E. Eckert, B. W. Sullivan, B. A. Hungate, J. P. Kaye, S. C. Hart, G. W. Koch, and A. Finkral (2010), Carbon and water fluxes from ponderosa pine forests disturbed by wildfire and thinning, *Ecol. Appl.*, *20*(3), 663–683, doi:10.1890/09-0934.1.

Ellis, A. W., T. W. Hawkins, R. C. Balling Jr., and P. Gober (2008), Estimating future runoff levels for a semi-arid fluvial system in central Arizona, USA, *Clim. Res.*, *35*(3), 227–239, doi:10.3354/cr00727.

Ellis, C. R., J. W. Pomeroy, T. Brown, and J. MacDonald (2010), Simulation of snow accumulation and melt in needleleaf forest environments, *Hydrol. Earth Syst. Sci.*, *14*, 925–940.
Essery, R. (2015), A factorial snowpack model (FSM 1.0), *Geosci. Model Dev.*, *8*(12), 3867–3876.
Essery, R., J. Pomeroy, J. Parviainen, and P. Storck (2003), Sublimation of snow from coniferous forests in a climate model, *J. Clim.*, *16*(11), 1855–1864, doi:10.1175/1520-0442(2003)016<1855:SOSFCF>2.0.CO;2.
Fassnacht, S. R., S. R. Helfrich, D. J. Lampkin, K. A. Dressler, R. C. Bales, E. B. Halper, D. Reigle, and B. Imam (2001), Snowpack modelling of the Salt Basin with water management implications, paper presented at Proceedings of The Western Snow Conference, Sun Valley, ID.
Foken, T., and B. Wichura (1996), Tools for quality assessment of surface-based flux measurements, *Agric. For. Meteorol.*, *78*(1-2), 83–105.
Ganey, J. L., and S. C. Vojta (2011), Tree mortality in drought-stressed mixed-conifer and ponderosa pine forests, Arizona, USA, *For. Ecol. Manage.*, *261*, 162–168.
Gelfan, A. N., J. W. Pomeroy, and L. S. Kuchment (2004), Modeling forest cover influences on snow accumulation, sublimation, and melt, *J. Hydrometeorol.*, *5*(5), 785–803, doi:10.1175/1525-7541(2004)005<0785:MFCIOS>2.0.CO;2.
Gesch, D., M. Oimoen, S. Greenlee, C. Nelson, M. Steuck, and D. Tyler (2002), The National Elevation Dataset, *Photogramm. Eng. Remote Sens.*, *68*(1), 5–11.
Gouttevin, I., M. Lehning, T. Jonas, D. Gustafsson, and M. Mölder (2015), A two-layer canopy model with thermal inertia for an improved snowpack energy balance below needleleaf forest (model SNOWPACK, version 3.2.1, revision 741), *Geosci. Model Dev.*, *8*(8), 2379–2398, doi:10.5194/gmd-8-2379-2015.
Groot Zwaaftink, C. D., R. Mott, and M. Lehning (2013), Seasonal simulation of drifting snow sublimation in alpine terrain, *Water Resour. Res.*, *49*, 1581–1590, doi:10.1002/wrcr.20137.
Gustafson, J. R., P. D. Brooks, N. P. Molotch, and W. C. Veatch (2010), Estimating snow sublimation using natural chemical and isotopic tracers across a gradient of solar radiation, *Water Resour. Res.*, *46*, W12511, doi:10.1029/2009WR009060.
Harpold, A. A., J. A. Biederman, K. Condon, M. Merino, Y. Korgaonkar, T. Nan, L. L. Sloat, M. Ross, and P. D. Brooks (2014), Changes in snow accumulation and ablation following the Las Conchas Forest Fire, New Mexico, USA, *Ecohydrology*, *7*(2), 440–452.
Hedstrom, N. R., and J. W. Pomeroy (1998), Measurements and modelling of snow interception in the boreal forest, *Hydrol. Processes*, *12*(10–11), 1611–1625, doi:10.1002/(SICI)1099-1085(199808/09)12:10/11<1611::AID-HYP684>3.0.CO;2-4.
Hood, E., M. Williams, and D. Cline (1999), Sublimation from a seasonal snowpack at a continental, mid-latitude alpine site, *Hydrol. Processes*, *13*(12–13), 1781–1797.
Jackson, S. I., and T. D. Prowse (2009), Spatial variation of snowmelt and sublimation in a high-elevation semi-desert basin of western Canada, *Hydrol. Processes*, *23*(18), 2611–2627.
Jin, S., L. Yang, P. Danielson, C. Homer, J. Fry, and G. Xian (2013), A comprehensive change detection method for updating the National Land Cover Database to circa 2011, *Remote Sens. Environ.*, *132*, 159–175.
Kaitera, P., and H. Teräsvirta (1972), Snow evaporation in South and North Finland 1969/79 and 1970/71, *Aqua Fennica*, *2*, 11–19.
Koeniger, P., J. A. Hubbart, T. Link, and J. D. Marshall (2008), Isotopic variation of snow cover and streamflow in response to changes in canopy structure in a snow-dominated mountain catchment, *Hydrol. Processes*, *22*(4), 557–566.
Koivusalo, H., M. Heikinheimo, and T. Karvonen (2001), Test of a simple two-layer parameterisation to simulate the energy balance and temperature of a snow pack, *Theor. Appl. Climatol.*, *70*, 65–79.
La Malfa, E. M., and R. Ryle (2008), Differential snowpack accumulation and water dynamics in aspen and conifer communities: Implications for water yield and ecosystem function, *Ecosystems*, *11*(4), 569–581.
Law, B. E., S. Van Tuyl, A. Cescatti, and D. D. Baldocchi (2001), Estimation of leaf area index in open-canopy ponderosa pine forests at different successional stages and management regimes in Oregon, *Agric. For. Meteorol.*, *108*, 1–14.
Lawler, R. R., and T. E. Link (2011), Quantification of incoming all-wave radiation in discontinuous forest canopies with application to snowmelt prediction, *Hydrol. Processes*, *25*(21), 3322–3331.
Liston, G. E., and D. K. Hall (1995), An energy-balance model of lake-ice evolution, *J. Glaciol.*, *41*(138), 373–382.
Liston, G. E., and K. Elder (2006a), A meteorological distribution system for high-resolution terrestrial modeling (MicroMet), *J. Hydrometeorol.*, *7*(2), 217–234.
Liston, G. E., and K. Elder (2006b), A distributed snow-evolution modeling system (SnowModel), *J. Hydrometeorol.*, *7*(6), 1259–1276, doi:10.1175/JHM548.1.
Luce, C. H., and D. G. Tarboton (2010), Evaluation of alternative formulae for calculation of surface temperature in snowmelt models using frequency analysis of temperature observations, *Hydrol. Earth Syst. Sci.*, *14*(3), 535–543.
Lundberg, A., and S. Halldin (2001), Snow interception evaporation. Review of measurement techniques, processes, and models, *Theor. Appl. Climatol.*, *70*(1–4), 117–133, doi:10.1007/s007040170010.
Lundquist, J. D., S. E. Dickerson-Lange, J. A. Lutz, and N. C. Cristea (2013), Lower forest density enhances snow retention in regions with warmer winters: A global framework developed from plot-scale observations and modeling, *Water Resour. Res.*, *49*, 6356–6370, doi:10.1002/wrcr.20504.
Mahat, V., and D. G. Tarboton (2014), Representation of canopy snow interception, unloading and melt in a parsimonious snowmelt model, *Hydrol. Processes*, *28*(26), 6320–6336, doi:10.1002/hyp.10116.
Mahat, V., D. G. Tarboton, and N. P. Molotch (2013), Testing above- and below-canopy representations of turbulent fluxes in an energy balance snowmelt model, *Water Resour. Res.*, *49*, 1107–1122, doi:10.1002/wrcr.20073.
Mahmood, T. H., and E. R. Vivoni (2014), Forest ecohydrological response to bimodal precipitation during contrasting winter to summer transitions, *Ecohydrology*, *7*, 998–1013.
Marks, D. G., M. Reba, J. Pomeroy, T. Link, A. Winstral, G. Flerchinger, and K. Elder (2008), Comparing simulated and measured sensible and latent heat fluxes over snow under a pine canopy to improve an energy balance snowmelt model, *J. Hydrometeorol.*, *9*(6), 1506–1522.
Marks, D., and J. Dozier (1992), Climate and energy exchange at the snow surface in the alpine region of the Sierra Nevada. 2. Snow cover energy balance, *Water Resour. Res.*, *28*(11), 3043–3054.
McDowell, N. G., S. White, and W. T. Pockman (2008), Transpiration and stomatal conductance across a steep climate gradient in the southern Rocky Mountains, *Ecohydrology*, *1*, 193–204.
Meromy, L., N. P. Molotch, M. W. Williams, K. N. Musselman, and L. M. Kueppers (2015), Snowpack-climate manipulation using infrared heaters in subalpine forests of the Southern Rocky Mountains, USA, *Agric. For. Meteorol.*, *203*, 142–157.
Mesinger, F., et al. (2006), North American Regional Reanalysis, *Bull. Am. Meteorol. Soc.*, *87*(3), 343–360.
Moeser, D., G. Mazzotti, N. Helbig, and T. Jonas (2016), Representing spatial variability of forest snow: Implementation of a new interception model, *Water Resour. Res.*, *52*, 1208–1226, doi:10.1002/2015WR017961.

Molotch, N. P., S. R. Fassnacht, R. C. Bales, and S. R. Helfrich (2004), Estimating the distribution of snow water equivalent and snow extent beneath cloud cover in the Salt-Verde River basin, Arizona, *Hydrol. Processes*, *18*(9), 1595–1611, doi:10.1002/hyp.1408.
Molotch, N. P., P. D. Blanken, M. W. Williams, A. A. Turnipseed, R. K. Monson, and S. A. Margulis (2007), Estimating sublimation of intercepted and sub-canopy snow using eddy covariance systems, *Hydrol. Processes*, *21*(12), 1567–1575, doi:10.1002/hyp.6719.
Molotch, N. P., P. D. Brooks, S. P. Burns, M. Litvak, R. K. Monson, J. R. McConnell, and K. Musselman (2009), Ecohydrological controls on snowmelt partitioning in mixed-conifer sub-alpine forests, *Ecohydrology*, *2*, 129–142.
Moreno, H. A., H. V. Gupta, D. D. White, and D. A. Sampson (2016), Modeling the distributed effects of forest thinning on the long-term water balance and streamflow extremes for a semi-arid basin in the southwestern US, *Hydrol. Earth Syst. Sci.*, *20*(3), 1241–1267.
Nakai, Y., T. Sakamoto, T. Terajima, K. Kitamura, and T. Shirai (1999), The effect of canopy-snow on the energy balance above a coniferous forest, *Hydrol. Processes*, *13*(14–15), 2371–2382.
Ohlanders, N., M. Rodriguez, and J. McPhee (2013), Stable water isotope variation in a central Andean watershed dominated by glacier and snowmelt, *Hydrol. Earth Syst. Sci.*, *17*(3), 1035–1050.
Perrot, D., N. P. Molotch, K. N. Musselman, and E. T. Pugh (2014), Modelling the effects of the mountain pine beetle on snowmelt in a sub-alpine forest, *Ecohydrology*, *7*, 226–241.
Pomeroy, J. W., J. Parviainen, N. Hedstrom, and D. M. Gray (1998), Coupled modelling of forest snow interception and sublimation, *Hydrol. Processes*, *12*(15), 2317–2337.
Pugh, E. T., and E. E. Small (2013), The impact of beetle-induced conifer death on stand-scale canopy snow interception, *Hydrol. Res.*, *44*(4), 644–657.
Reba, M. L., J. Pomeroy, D. Marks, and T. E. Link (2012), Estimating surface sublimation losses from snowpacks in a mountain catchment using eddy covariance and turbulent transfer calculations, *Hydrol. Processes*, *26*(24), 3699–3711.
Reba, M. L., D. Marks, T. E. Link, J. Pomeroy, and A. Winstral (2014), Sensitivity of model parameterizations for simulated latent heat flux at the snow surface for complex mountain sites, *Hydrol. Processes*, *28*(3), 868–881.
Rinehart, A. J., E. R. Vivoni, and P. D. Brooks (2008), Effects of vegetation, albedo, and solar radiation sheltering on the distribution of snow in the Valles Caldera, New Mexico, *Ecohydrology*, *1*, 253–270.
Rylov, S. P. (1969), Snow cover evaporation in the semi-desert zone of Kazakhstan, *Sel. Pap. Soviet Hydrol.*, *3*, 258–270.
Salzmann, N., and L. O. Mearns (2012), Assessing the performance of multiple regional climate model simulations for seasonal mountain snow in the Upper Colorado River Basin, *J. Hydrometeorol.*, *13*(2), 539–556.
Schmidt, R. A., and C. A. Troendle (1992), Sublimation of intercepted snow as a source of global water vapor. Presented at the 60th annual Western Snow Conference. Jackson Hole, Wyoming.
Schmidt, R. A., C. A. Troendle, and J. R. Meiman (1998), Sublimation of snowpacks in subalpine conifer forests, *Can. J. For. Res.*, *28*(4), 501–513.
Schotanus, P., F. T. M. Nieuwstadt, and H. A. R. De Bruin (1983), Temperature measurement with a sonic anemometer and its application to heat and moisture fluxes, *Boundary-Layer Meteorol.*, *26*(1), 81–93.
Seager, R., et al. (2007), Model projections of an imminent transition to a more arid climate in southwestern North America, *Science*, *316*(5828), 1181–1184.
Serreze, M. C., M. P. Clark, R. L. Armstrong, D. A. McGinnis, and R. S. Pulwarty (1999), Characteristics of the western United States snowpack from Snowpack Telemetry (SNOTEL) data, *Water Resour. Res.*, *35*(7), 2145–2160, doi:10.1029/1999WR900090.
Sexstone, G. A., D. W. Clow, D. I. Stannard, and S. R. Fassnacht (2016), Comparison of methods for quantifying surface sublimation over seasonally snow-covered terrain, *Hydrol. Processes*, *30*, 3373–3389, doi:10.1002/hyp.10864.
Sheppard, P. R., A. C. Comrie, G. D. Packin, K. Angersbach, and M. K. Hughes (2002), The climate of the US Southwest, *Clim. Res.*, *21*(3), 219–238.
Sicart, J. E., J. W. Pomeroy, R. L. H. Essery, J. Hardy, T. Link, and D. Marks (2004), A sensitivity study of daytime net radiation during snowmelt to forest canopy and atmospheric conditions, *J. Hydrometeorol.*, *5*(5), 774–784.
Sogachev, A., U. Rannik, and T. Vesala (2004), Flux footprints over complex terrain covered by heterogeneous forest, *Agric. For. Meteorol.*, *127*, 143–158.
Storck, P., D. P. Lettenmaier, and S. M. Bolton (2002), Measurement of snow interception and canopy effects on snow accumulation and melt in a mountainous maritime climate, Oregon, United States, *Water Resour. Res.*, *38*(11), 1223, doi:10.1029/2002WR001281.
Strasser, U., and T. Marke (2010), ESCIMO.spread—A spreadsheet-based point snow surface energy balance model to calculate hourly snow water equivalent and melt rates for historical and changing climate conditions, *Geosci. Model Dev.*, *3*(2), 643–652.
Strasser, U., M. Bernhardt, M. Weber, G. E. Liston, and W. Mauser (2008), Is snow sublimation important in the alpine water balance? *Cryosphere*, *2*(1), 53–66.
Strasser, U., M. Warscher, and G. E. Liston (2011), Modeling snow-canopy processes on an idealized mountain, *J. Hydrometeorol.*, *12*(4), 663–677, doi:10.1175/2011JHM1344.1.
Suzuki, K., and Y. Nakai (2008), Canopy snow influence on water and energy balances in a coniferous forest plantation in northern Japan, *J. Hydrol.*, *352*(1–2), 126–138.
Suzuki, K., J. Kubota, Y. Zhang, T. Kadota, T. Ohata, and V. Vuglinsky (2006), Snow ablation in an open field and larch forest of the southern mountainous region of eastern Siberia, *Hydrol. Sci. J.*, *51*(3), 465–480.
Suzuki, K., Y. Kodama, T. Nakai, G. E. Liston, K. Yamamoto, T. Ohata, Y. Ishii, A. Sumida, T. Hara, and T. Ohta (2011), Impact of land-use changes on snow in a forested region with heavy snowfall in Hokkaido, Japan, *Hydrol. Sci. J.*, *56*(3), 443–467.
Suzuki, K., G. E. Liston, and K. Matsuo (2015), Estimation of continental-basin-scale sublimation in the Lena River basin, Siberia, *Adv. Meteorol.*, *2015*, doi:10.1155/2015/286206.
Svoma, B. M. (2016), Difficulties in determining snowpack sublimation in complex terrain at the macroscale, *Adv. Meteorol.*, *2016*, doi:10.1155/2016/9695757.
Svoma, B. M., R. C. Balling Jr., and A. W. Ellis (2010), Analysis of soil moisture trends in the Salt River watershed of central Arizona, *Theor. Appl. Climatol.*, *102*(1), 159–169.
Thorpe, A. D., and B. J. Mason (1966), The evaporation of ice spheres and ice crystals, *Br. J. Appl. Phys.*, *17*(4), 541–548.
Van Den Broeke, M. R. (1997), Spatial and temporal variation of sublimation on Antarctica: Results of a high-resolution general circulation model, *J. Geophys. Res.*, *102*(25), 29,765–29,777, doi:10.1029/97JD01862.
Vivoni, E. R., A. Rango, C. A. Anderson, N. A. Pierini, A. P. Schreiner-Mcgraw, S. Saripalli, and A. S. Laliberte (2014), Ecohydrology with unmanned aerial vehicles, *Ecosphere*, (10), 5.
Yamazaki, T., H. Yabuki, and T. Ohata (2007), Hydrometeorological effects of intercepted snow in an eastern Siberian taiga forest using a land-surface model, *Hydrol. Processes*, *21*(9), 1148–1156.